Alvus: A Reconfigurable 2-D Wireless Charging System

KAZUNOBU SUMIYA, The University of Tokyo, Japan
TAKUYA SASATANI, The University of Tokyo and JSPS Research Fellow, Japan
YUKI NISHIZAWA, The University of Tokyo, Japan
KENJI TSUSHIO, The University of Tokyo, Japan
YOSHIAKI NARUSUE, The University of Tokyo, Japan
YOSHIHIRO KAWAHARA, The University of Tokyo, Japan

Wireless charging pads such as Qi are rapidly gaining ground, but their limited power supply range still requires precise placement on a specific point. 2-D wireless power transfer (WPT) sheets consisting of coil arrays are one well-known counterpart to extend this range. However, these approaches require custom-made designs by expert engineers; what we need is a WPT system that can be reconfigured by simply placing ready-made modules on the intended surface (*e.g.*, table, floor, shelf board, etc). In this paper, we present "Alvus", a reconfigurable 2-D WPT system which enables such simple construction of WPT surfaces. Our system is based on multihop WPT that composes "virtual power cords" and consists of three types of ready-made resonator modules: (i) transmitter, which outputs energy, (ii) relays, which pass energy down to the next module, and (iii) receivers, which receive energy and charge the loads. We show that power can be transferred efficiently (over 25%) within a range of 19.6 m^2 using a single transmitter. We implemented an end-to-end WPT system and demonstrated that Alvus is capable of intuitive construction/reconfiguration of WPT surfaces, as well as automatically deciding the power routes based on the sensed information (*e.g.*, receiver location, module placement, obstructive objects).

CCS Concepts: • **Human-centered computing → Ubiquitous and mobile computing systems and tools**; • **Hardware → Wireless devices**.

Additional Key Words and Phrases: Wireless power transfer; Multihop WPT; Reconstructable Charging Area; Dynamic Power Routing.

ACM Reference Format:
Kazunobu Sumiya, Takuya Sasatani, Yuki Nishizawa, Kenji Tsushio, Yoshiaki Narusue, and Yoshihiro Kawahara. 2019. Alvus: A Reconfigurable 2-D Wireless Charging System. *Proc. ACM Interact. Mob. Wearable Ubiquitous Technol.* 3, 2, Article 68 (June 2019), 29 pages. https://doi.org/10.1145/3332533

1 INTRODUCTION

The Internet of Things, which aims to weave computation into everyday life by embedding numerous computers in surrounding objects, is rapidly gaining ground. In conjunction with this trend, an abundance of power cords

Authors' addresses: Kazunobu Sumiya, The University of Tokyo, 7-3-1 Hongo, Bunkyo-ku, Tokyo, 113-8656, Japan, sumiya@akg.t.u-tokyo.ac.jp; Takuya Sasatani, The University of Tokyo and JSPS Research Fellow, 7-3-1 Hongo, Bunkyo-ku, Tokyo, 113-8656, Japan, sasatani@akg.t.u-tokyo.ac.jp; Yuki Nishizawa, The University of Tokyo, 7-3-1 Hongo, Bunkyo-ku, Tokyo, 113-8656, Japan, nishizawa@akg.t.u-tokyo.ac.jp; Kenji Tsushio, The University of Tokyo, 7-3-1 Hongo, Bunkyo-ku, Tokyo, 113-8656, Japan, tsushio@akg.t.u-tokyo.ac.jp; Yoshiaki Narusue, The University of Tokyo, 7-3-1 Hongo, Bunkyo-ku, Tokyo, 113-8656, Japan, narusue@mlab.t.u-tokyo.ac.jp; Yoshihiro Kawahara, The University of Tokyo, 7-3-1 Hongo, Bunkyo-ku, Tokyo, 113-8656, Japan, kawahara@akg.t.u-tokyo.ac.jp.

2474-9567/2019/6-ART68 $15.00
https://doi.org/10.1145/3332533

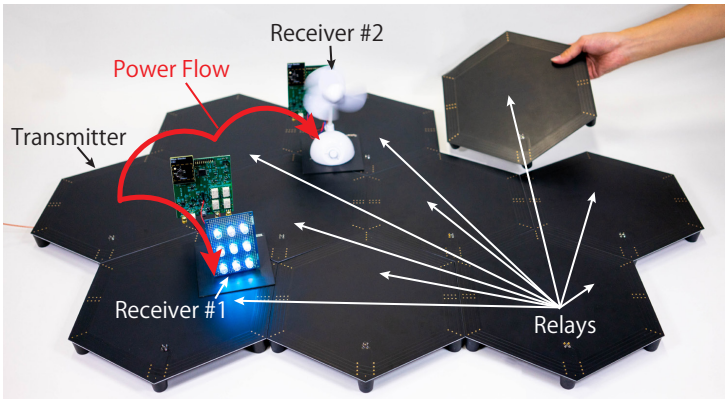

Fig. 1. Alvus enables users to retrofit everyday surfaces (*e.g.*, table, shelf board, floor, etc.) into wireless charging surfaces by simply arranging our ready-made modules. The transmitter module is the only module which is powered by wires, the relay modules construct the route of power delivery by enabling/disabling the relay effect, and the receiver modules supply the received power to the load.

causing clutter has become a familiar sight in typical home and office environments; this not only spoils the appearances but also makes it difficult to arrange mobile devices (*e.g.*, sensors, cameras, displays, and robots) in intended layouts. Although wireless power transfer (WPT) standards such as Qi [9, 50] appeared, these chargers only provide a point-to-point solution, which still requires users to place devices at a specific point and limits mobility. As many electrical devices are placed or hung on surfaces such as a tabletop, walls, and the floor, augmenting these surfaces for power supply is probably the most rational and natural way to eliminate power codes in daily environments.

In this paper, we propose Alvus, a reconfigurable system that enables the accommodation of wireless power capability on floors, tables, and walls; using our system, end-users can retrofit existing 2-D surfaces by simply arranging ready-made modules. Unlike existing 2-D power supply sheets [7, 27, 38, 39], Alvus can dynamically configure virtual paths through which electric power passes on the 2-D plane, as shown in Fig. 1.

The features of Alvus are as follows:

- **Easy augmentation of the surface:** All the users have to do is to arrange Alvus modules so that they fit into the intended surface.
- **Wireless interconnection between modules:** Each Alvus module has no physical connection and is charged wirelessly; unlike typical coil array systems, there is no need to wire modules together.
- **Automatic generation of virtual power cords:** The system automatically detects the placement of the modules, finds the receivers, and directs energy to the receivers. Additional protocols, such as detouring troublesome objects and avoiding human bodies to prevent unnecessary electromagnetic field exposure can also be developed on Alvus.

The key technology underlying in Alvus is multihop WPT, which is a technology based on magnetic resonant coupling and has the potential of dynamically configuring the energy route. Existing WPT methods are classified into *far-field* and *near-field* systems. Although many wide-range wireless power supply systems using far-field (*e.g.*, microwave) WPT methods have been proposed [6, 44], such systems can only transmit several milli-watts at most, due to health and safety concerns. Thus, to efficiently provide several watts of power near surfaces such as floors and walls, it is necessary to use near-field WPT systems.

Currently, the most successful near-field wireless charging standard is the Qi standard. Qi is based on inductive coupling WPT, which is highly efficient when perfectly aligned, although the covering range forms a single "point". It may be possible to assort a bunch of Qi transmitters and form a dense array; however, since this is still a set of "points", it requires an extremely dense placement, an impractical number of coils, and an accordingly impractical amount of wiring to form a wide surface. Magnetic resonant coupling-based WPT is also a near-field method, which transfers energy via the inductive link between coil resonators [18]. This method has high efficiency in mid-range and therefore brings about a degree of positional freedom [33]; however, as this method is based on near-field magnetic field, the transmission range is still limited to the proximity of the transmitter. This issue can be solved by constructing arrays of transmitters. For example, 2-D transmitter array systems [39, 48] and phased array WPT systems [11, 40, 52] have extended the capability of WPT to surfaces. However, these transmitter arrays usually need to be interconnected by wires that supply power to each transmitter. Therefore, the shape cannot be modified easily, and an order-made design is premised, resulting in a high-cost and permanent system installation. In contrast, "multihop" WPT, which uses multiple "relay" resonators to extend the power transmission range, is a technology that interconnects these elements within 2-D arrays in a wireless manner. Instead of directing power to each transmitter through wires, power can be made to "hop" through the inductive coupling between relay resonators; consequently, wired interconnection within the 2-D array becomes unnecessary. This technology has the promise of intuitive construction/reconfiguration of WPT surfaces, by simply placing ready-made modules on the intended surface.

Although the concept and theory of multihop WPT has been investigated, no prior study has presented a full *end-to-end* 2-D multihop WPT system. While it is clear that multihop WPT can bring about unfathomable benefits in terms of construction/reconfiguration, we notice that many unavoidable challenges exist. Even imagining a simple procedure such as delivering power to a given coordinate, multihop 2-D WPT systems need to figure out the location of each module and know which module to activate, since the modules can be naturally shuffled, whereas typical 2-D arrays can simply switch on the transmitter based on the fixed configuration. Such difficulties are present everywhere in the system architecture, which brings about difficulty not only in solving each problem but also in the integration of all solutions. To overcome these challenges, we first organize the primitive functions needed and then break them down into physical implementations. The key challenges we address in this process are the following: (a) detection and map generation of the modules composing a 2-D array (b) receiver proximity detection, (c) dynamic power routing, (d) obstacle object detection, and (e) power distribution to each module. Finally, all these functions are integrated in Alvus, which enables our reconfigurable and dynamic power routing concept.

The contributions of this work can be summarized as follows:

(1) **System design of a reconfigurable 2-D WPT system**: We organized the required operation procedures into four components, broke them down into six primitive functions, and integrated them into a single system.
(2) **End-to-end system implementation**: We designed and implemented resonator modules of Alvus as well as its software and integrated it into an automated end-to-end system.
(3) **Comprehensive system evaluation and demonstration**: We conducted comprehensive evaluations (*e.g.*, energy efficiency, detection sensitivity, time overhead, etc.) to explore the performance of our system. We also demonstrated the capabilities of our system by building three applications: a wireless charging desk, a wireless charging shelf, and a wirelessly powered robot.

In section 2, related works on WPT are revisited. Section 3 introduces the system design of Alvus. The technical challenges and implementation details are explained in section 4. Evaluation results of the system are shown in section 5. Finally, potential applications and limitations of this system are discussed in section 6.

2 BACKGROUND AND RELATED WORKS

In this section, we provide a brief introduction to existing works on WPT and explain our motivation behind using multihop WPT for our solution.

2.1 Microwave Power Transfer

WPT using far-field microwaves is one of the most intensely studied methods in WPT [2, 3, 6, 44]. The transmitter antenna generates microwaves and the receiver antennas receive it; this is identical to the physical layer of typical wireless communication (*i.e.*, cellular, Wi-Fi, Bluetooth, etc). Due to the nature of far-field waves, the power transfer range of this method is known to be long in ideal setups (*i.e.*, large antenna arrays with numerous elements, sophisticated control systems, etc); therefore, applications such as space solar power station (SSPS) [23, 35, 45] and ubiquitous WPT [46] have been explored. In typical microwave power transfer systems, the footprint of the transmitter/receiver needs to be comparable to the wavelength, therefore the typical frequency band used in this method is around a GHz. This brings about low efficiency in the AC-to-DC and DC-to-AC conversion, and moreover, the SAR per transmitted power tends to be typically high in these frequencies. Consequently, the amount of power that can be delivered within regulatory guidelines is low. Another research trend on microwave power transfer is ambient energy harvesting, wherein power is harvested from existing microwaves such as TV broadcasts and Wi-Fi to drive battery-less sensors [10, 15, 29, 34, 42, 49]. However, the power levels of these systems are limited to several microwatts of power as ambient microwave signals are inherently small. Alvus aims to deliver power over several watts; therefore, microwave power transfer is unsuitable for our proposal.

2.2 Inductive Power Transfer

Inductive power transfer is a method that transfers power via the inductive link between coils [8]. This method is used in the commercially successful Qi standard [50]. Although inductive WPT is known for its high efficiency and is considered safe, the typical transfer distance is short (*e.g.*, up to a centimeter), which limits mobility. Moreover, its efficiency drastically decreases when the transmitter coil and receiver coil are misaligned, so power can only be delivered to a single point. Some systems use 2-D transmitter coil arrays to overcome this issue. Such systems connect many transmitters to a power source via many switches and selectively activate the transmitter in proximity of the receiver [39, 48]. While these systems can effectively direct energy to the intended position, the shape of the coil array cannot be freely designed nor reconfigured by the users. This opposes our vision of the interactive and instant fabrication of WPT surfaces.

2.3 Magnetic Resonant Coupling Wireless Power Transfer

Wireless power transfer based on magnetic resonant coupling (WPT-MRC) is a method introduced by Kurs *et al.* in 2007 [18]. From the viewpoint of circuit theory, WPT-MRC is an extension of inductive WPT, although it uses a pair of inductively coupled high-Q (typically over 100) *LC* resonators instead of coils. These two methods are identical in the point that energy is sent via the inductive link [14, 31, 32]. WPT-MRC has the promise of high efficiency over mid-range (*e.g.*, up to a meter) power delivery and misaligned conditions; moreover, many studies based on SAR have demonstrated that this method is relatively safe for the human body [5, 21, 22, 43].

The relatively good misalignment tolerance of WPT-MRC motivated its use in applications such as charging implanted devices [53], bio-monitoring sensors for animals [24], and robotics [1, 30]. However, the power transfer range using this method is still around the value of the diameter of the transmitter/receiver coil, which means the power delivery range still remains within the proximity of a single point [8]. Therefore, many attempts have been made to extend this range into 2-D surfaces and 3-D volumes.

Typical 2-D systems are constructed by arranging transmitter resonators into arrays; operations on these arrays can be roughly divided into (a) selective activation, which activates the transmitter in proximity of the

receiver [12, 20, 25, 47] and (b) phased array-inspired operation, which adjusts the gain/phase of each transmitter element to form a constructive interference at the receiver [11, 16, 40, 52]. In both (a) and (b), it is premised that the transmitter elements are wired to the central power source, which limits shape modification. As a countermeasure to this issue, Takahashi *et al.* proposed a "cuttable" WPT sheet, which can be modified into various shapes [47]. However, many rules for cutting still exist; moreover, it is based on irreversible modification. The learning threshold for users still remain high and the shape cannot be “re”configured in many cases.

Another trend is 3-D systems that employ cavity-based resonators [4, 36, 37]. Although 3-D systems are useful, current methods require a full renovation of the room. Furthermore, it is beneficial to keep the magnetic field only where necessary (*i.e.*, where the target device is), especially for high-power applications. Therefore, our belief is that 2-D systems, which have low installation cost and can focus the electromagnetic field on a surface (*i.e.*, floor, table, wall, or any surface that devices are placed on) are still necessary, even while 3-D systems are developed further.

2.4 Multihop Wireless Power Transfer

Multihop WPT is a method based on WPT-MRC, which uses the “multihop” phenomenon. When passive *LC* resonators are placed within a magnetic field oscillating at its resonant frequency (*e.g.*, field generated by transmitter resonator), the placed *LC* resonator works as a tank of reactive energy and generates a magnetic field distribution in proximity to itself. This phenomenon makes the magnetic field seem to be “repeated” by the placed *LC* resonators (*i.e.*, relay resonators) and consequently, the range that the oscillating magnetic field reaches (*i.e.*, the power transfer range) is extended [see Fig. 2(b)]. Moreover, the number of “hops” is not limited to a specific number; by laying multiple relay resonators so that they form a line (or a polyline), the range of the power transfer can be extended accordingly.

Prior studies have investigated the technical aspects of multihop WPT. An analysis of maximum efficiency conditions when the positions of relay coils are varied is a common interest [54, 55]. The effect of coupling between non-adjacent coils (*i.e.*, cross-coupling) is investigated as well since it degrades the transfer efficiency at a given operation frequency [19]. It is also known that the impedance matching conditions depend on the number of hops from the transmitter to the receiver [51]; a study established an impedance matching method by adjusting the distance between hops to gain consistent input impedance in any-hop systems [27]. There are also works on receiver localization in a 2-D multihop system [7], and simultaneous power and data transfer on the multihop WPT channel [17].

One of the concepts Alvus uses is “virtual power cords” on 2-D surfaces [13]; by packing resonators on 2-D surfaces and activating/deactivating the “hop” effect of each relay resonator, a “virtual power cord” from the transmitter to the receiver can be configured. Shi *et al.* proposed a multihop WPT system using a planar array of relay resonators and investigated its effect on the system (*e.g.*, shift in optimal driving frequency, power efficiency, etc) when the activated relay coils are varied [41]. While this is similar to our concept, this is only an initial investigation of AC-to-AC performance; investigation at system level and implementation are still necessary to achieve the concept of Alvus.

3 SYSTEM OVERVIEW

In a big picture, the objective of “Alvus” is to provide a system that the user can construct and re-configure 2-D WPT surfaces, by simply laying ready-made modules on the intended surface. To break down this concept into a physical implementation, we need a technology that (i) enables power delivery over a long distance from a single power source and (ii) allows the power to be directed to the RX thorough untethered modules (*i.e.*, the system can work without a physical connection between Alvus modules, such as “carpet tiles”). (i) is essential for enabling a wide power delivery range since RF power sources are typically expensive and resonator size is restricted by

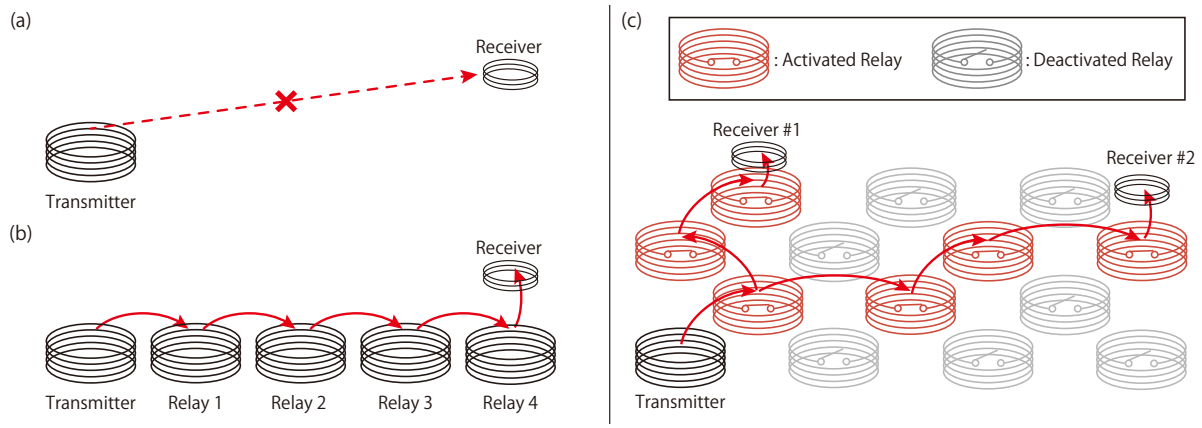

Fig. 2. Overview of multihop WPT. (a) WPT systems with one transmitter and one receiver. The receiver cannot receive power since the power delivery range of typical near-field WPT systems are limited to the proximity of the transmitters. (b) 1-D multihop WPT. The linearly aligned resonators deliver power from the transmitter to the receiver wirelessly. These resonator modules "relay" power to adjacent resonator modules and finally passes power down to the RX resonator module. (c) 2-D multihop WPT. The surface is packed with programmable (*i.e.*, can enable/disable the relay effect) resonator modules. The route for power delivery can be dynamically configured through enabling/disabling the relay effect of each module.

effects introduced by wavelength, and (ii) is a requirement that enables simple and intuitive construction of the functional surface (*i.e.*, the user is not required to perform explicit operations such as interconnecting the modules). From this context, we concluded that "multihop" WPT [see section 2.4] is the key technology to enable our concept.

3.1 Key Concept and the Primitive Building Blocks of Alvus

While the power delivery range of a typical WPT systems is limited to the proximity of the TX resonator [see Fig. 2(a)], typical "multihop" WPT extends this range to a single fixed line formed by *LC* resonator modules [see Fig. 2(b)]. These *LC* resonators are tuned to a specific resonant frequency f_0 under series resonance condition:

$$\omega_0 = 2\pi f_0 = \frac{1}{\sqrt{LC}} \tag{1}$$

These *LC* resonator modules "relay" power to adjacent *LC* resonator modules and finally pass power down to the RX resonator module. Here, the key idea of Alvus is to construct a surface packed with programmable (*i.e.*, can enable/disable the relay effect) *LC* resonator modules and dynamically configure the power delivery route by enabling/disabling the relay effect of each module, as shown in Fig. 2(c). Since this power route is virtual and re-programmable, receivers placed anywhere on the 2-D surface can be powered. Based on this idea, we provide three types of resonator modules, which work as building blocks for Alvus:

(1) **Transmitter module**: The only module that is connected to the power source. When an RF current oscillating at the resonant frequency f_0 is fed into this module, a magnetic field is generated, which supplies energy to adjacent relay resonator modules.
(2) **Relay module**: The module that relays power from the previous module to the next module [see Fig. 2]. The relay effect can be enabled/disabled by toggling the *LC* resonator between short (enable)/open (disable) state.

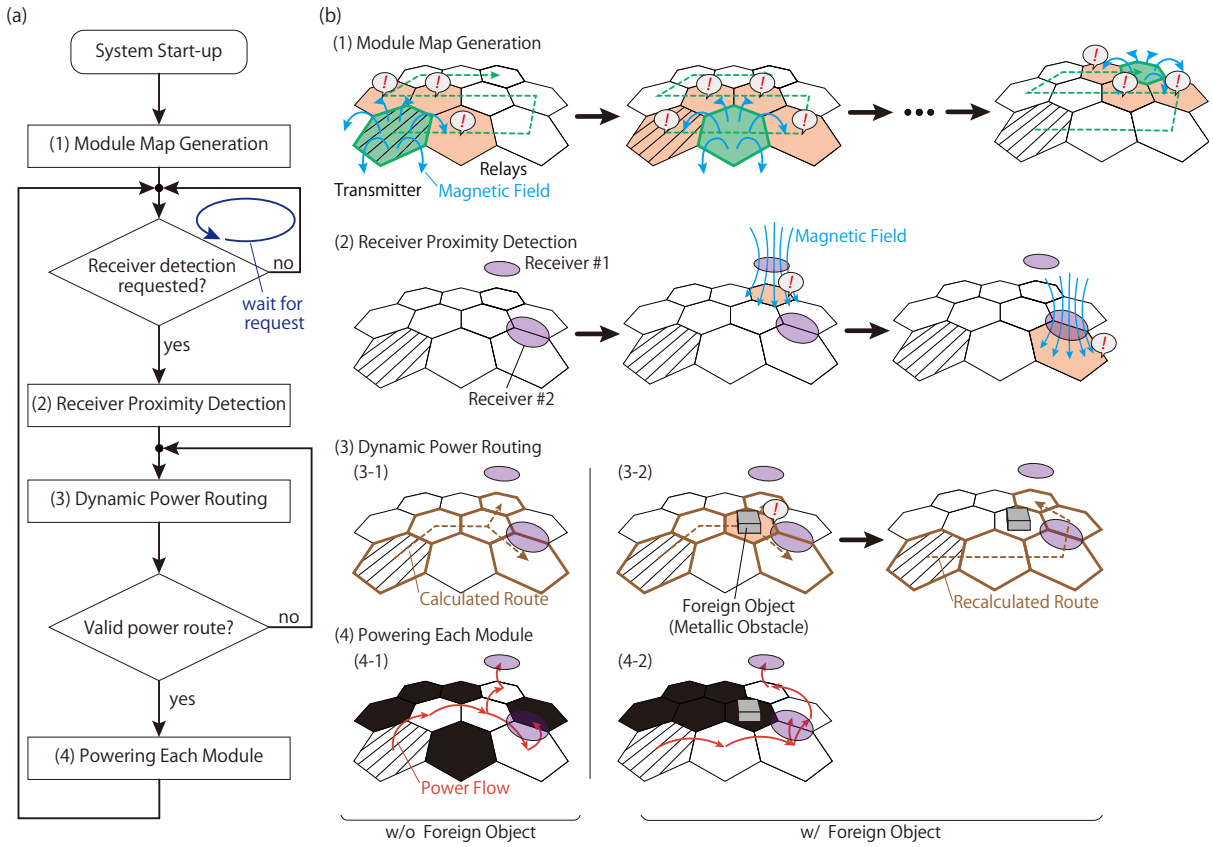

Fig. 3. (a) The operational flow diagram of Alvus. (b) The visualized operation flow.

(3) **Receiver module**: The module that receives power from the transmitter via the nearest relay module. The received power is rectified and converted to DC, which is supplied to the load device.

All modules can wirelessly communicate with and can be controlled by the central control unit. We assume a setup where the transmitter module equipped together with the central control unit is placed near the power outlet, and the relay modules are placed around the transmitter module to freely extend the WPT-enabled area to an intended shape.

3.2 Design Objectives and Operation Procedure

To construct a reconfigurable 2-D WPT system based on multihop WPT, we set the design objectives of Alvus as the automatic execution of the following functions:

(1) **Module Map Generation**: Detect the topology of the placement of the modules, which form a 2-D surface.
(2) **Receiver Proximity Detection**: Detect the position of the receiver when it is on the constructed WPT surface.

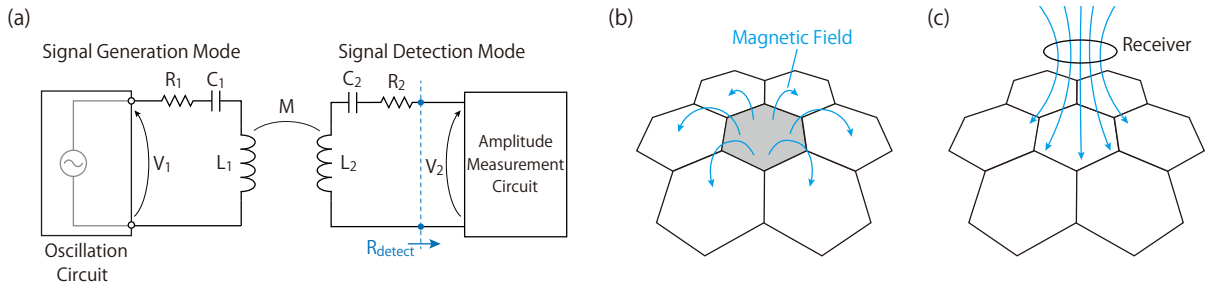

Fig. 4. Overview of the resonator detection mechanism. This is used for both the module map generation and receiver proximity detection. (a) Equivalent circuit. One module is in signal generation mode and the other modules are in signal detection mode. The signal generation module generates a magnetic field oscillating at 6.78 MHz, and the signal detection module "listens" to this generated field by monitoring the amplitude of the induced voltage. (b) The relay detection process. The gray module (signal generation mode [(a), left]) generates a magnetic field and the other modules (signal detection mode [(a), right]) listen to it. The listening modules can determine if the gray module is adjacent or not from the signal strength. (c) The receiver proximity detection process. The receiver works in signal generation mode and the other modules (*i.e.*, transmitter and relays) detect the generated magnetic field through the induced voltage. From the detected voltage values, the module that is most strongly coupled to the receiver can be determined.

(3) **Dynamic Power Routing**: Determine the route, validate that the route still works (*i.e.*, does not have obstructive objects), and configure the route by updating the state of each module, so that power is efficiently directed to the RX.
(4) **Powering Each Module**: Deliver power to each unit from the single RF power source in a wireless and efficient manner.

Based on these functions, we designed the operational procedure as shown in Figure 3. The basic mechanisms used for these functions are described as follows.

3.2.1 Module Map Generation. The initialization process starts with detecting the positions of the transmitter and the relay modules, and then proceeds to generate a topological map. First, the central control unit commands a single module (module in "signal generation mode") to generate a magnetic field oscillating at the resonant frequency f_0 and the remaining modules (modules in "signal detection mode") to measure the induced voltage [see Fig. 4(a)]. Assuming that the impedance of the module in signal detection mode is high enough and therefore non-ideal effects such as cross-coupling can be neglected, the voltage induced in the module in signal detection mode $|V_2|$ can be formulated as follows [7]:

$$|V_2| = \frac{\omega_0 M R_{\text{detect}}}{\left(R_1 + \frac{1}{j\omega_0 C_1} + j\omega_0 L_1\right)\left(R_2 + \frac{1}{j\omega_0 C_2} + j\omega_0 L_2 + R_{\text{detect}}\right) + (\omega_0 M)^2}|V_1| = \frac{\omega_0 M R_{\text{detect}}}{R_1\left(R_2 + R_{\text{detect}}\right) + (\omega_0 M)^2}|V_1| \quad (2)$$

Here, M is the mutual inductance between the modules in signal generation mode and signal detection mode; this is the parameter we intend to extract in this procedure. V_1 and R_{detect} are the voltage applied to the module in signal generation mode and the input impedance of the measurement circuit of the module in detecting mode, respectively. By adopting high-impedance voltage measurement circuits such as opamp-based peak-detectors and using the resulting relationship of $R_1(R_2 + R_{\text{detect}}) \gg (\omega_0 M)^2$ and $(R_2 + R_{\text{detect}}) \sim R_{\text{detect}}$, equation 2 can be

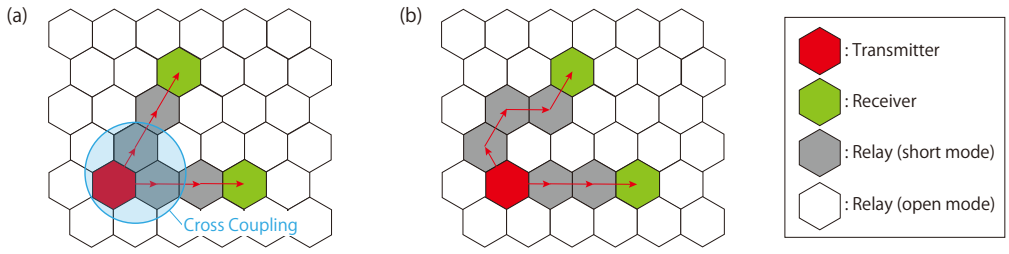

Fig. 5. Examples of the power supply route from the transmitter (red) to the two receivers (green). (a) Improper routing. The cross-coupling (shown in the blue circle) degrades power transmission efficiency. (b) Proper routing generated by Alvus, which avoids cross-coupling.

approximated as follows:

$$|V_2| \sim \frac{\omega_0 M R_{\text{detect}}}{R_1 (R_2 + R_{\text{detect}})} |V_1| \tag{3}$$

$$\sim \frac{\omega_0 M}{R_1} |V_1| \tag{4}$$

Since $\omega_0, R_1, |V_1|$ are all known parameters, M can be extracted using the measured value of $|V_2|$; M has a positive correlation with coupling between the modules, therefore this value determines the "closeness in the terms of magnetic coupling". By repetitively performing this procedure so that every module gets to be in the signal generation mode [see Fig. 3(b-1)], a full map of modules, which is an non-directed graph, can be obtained.

3.2.2 Receiver Proximity Detection. The voltage supplied to the receiver is continuously monitored while supplying power; if this voltage falls below the pre-defined threshold value, a request for receiver detection is sent to the central control unit. This voltage drop happens when (i) the receiver module is placed on the WPT surface for the first time (*i.e.*, the route needs to be initialized) or when (ii) the receiver module is moved (*i.e.*, the route needs to be changed).

The receiver proximity detection procedure uses the same mechanism as the map generation procedure. When the receiver proximity detection is requested, the central control unit commands the receiver module to work in signal generation mode, while the transmitter and relay modules work in signal detection mode [see Fig. 4(c)]. From the detected voltage values, the module that is most strongly coupled to the receiver can be found. Finding the most strongly coupled module is essential for WPT, whereas estimating the "physical" position of the receiver is not; the figure of merit that directly corresponds to WPT efficiency is coupling.

3.2.3 Dynamic Power Routing. Now that we have obtained the map of the transmitter/relay modules and localized the receiver module, the central control unit can generate a route for multihop power delivery and configure the relay modules so that the path is physically established. We set the basic requirements for the route generation as follows:

- Cross-coupling [19] is avoided [see Fig. 5].
- The route has no cumbersome foreign objects (*i.e.*, objects that induce loss) on it [see Fig. 3(b-3-2)].

The first requirement is important as cross-coupling often results in non-desired shifts in the resonant frequency; this causes difficulty in controlling the system as well as a decrease in power transfer efficiency in many cases.

As for the second requirement, we note that when there is a metallic object on the constructed power route, eddy current occurs, which induces a magnetic field that (a) cancels out the incident field and also (b) causes copper loss; these are factors that degrade transfer efficiency. As a countermeasure, Alvus automatically detects

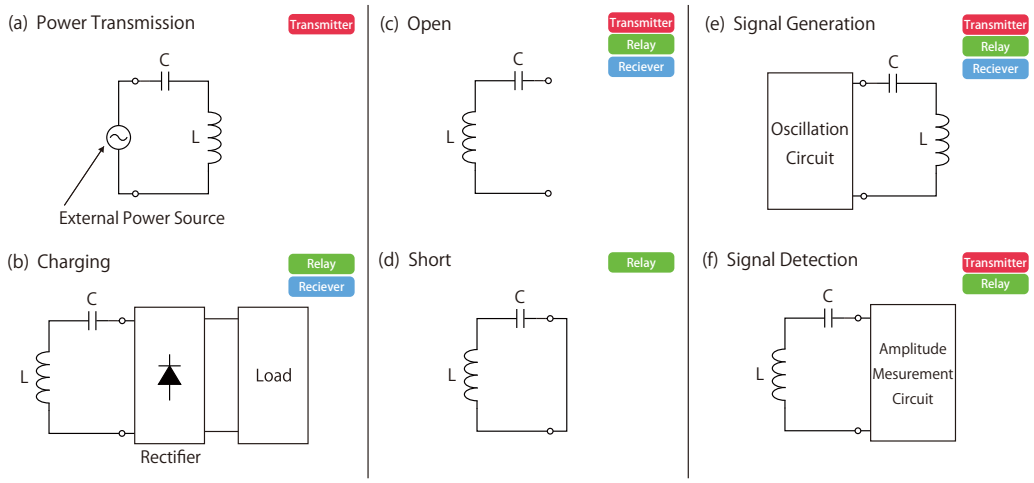

Fig. 6. Six required functions of Alvus modules.

the metallic objects on the power route and regenerates a power route that takes a detour to avoid the object when metallic objects exist. The foreign object detection process is conducted in the same manner as the map generation process; our system detects the foreign objects by measuring $|V_2|$, which is induced by the magnetic field that the signal generation mode generates [see Fig. 4(a)]. If a foreign object that could degrade transmission efficiency exists near the module in signal generation mode (*i.e.*, the primary side), eddy current occurs, which makes the mutual inductance M smaller and the resistance R_1 larger, as mentioned above. Consequently, the induced voltage $|V_2|$ in the Eq. 4 decreases; then, if there is an obvious decrease in voltage compared to the value during the previous map generation process, the system recognizes that a foreign object exists on the module in signal generation mode. Note that we assume there is no foreign object during the initial map generation process; this procedure is conducted immediately after the users finish the installation of the modules, so the users are required to exclude foreign objects during this initialization.

3.3 Required Functions of Modules

Now that the operation procedure is defined and the mechanism for each process is considered, we discuss the primitive functions that the modules should possess. The six functions listed below and shown in Fig. 6 are the functions necessary to enable the aforementioned operation procedure:

(a) Power Transmission: Control the ON/OFF of the RF power input. (*Required in: Transmitter module.*)
(b) Charging: Receive power via the ambient magnetic field, rectify, and supply power to the battery and the load. (*Required in: Relay and receiver module.*)
(c) Open: Make the impedance of the resonator high and disable the multihop effect. This minimizes interference with nearby modules. (*Required in: All modules.*)
(d) Short: Make the impedance of the resonator low and enable the multihop effect. (*Required in: Relay module.*)
(e) Signal Generation: Generate the magnetic field for map generation, receiver proximity detection, and foreign object detection. (*Required in: All modules.*)
(f) Signal Detection: Detect the magnetic field for map generation , receiver proximity detection, and foreign object detection. (*Required in: Transmitter and relay module.*)

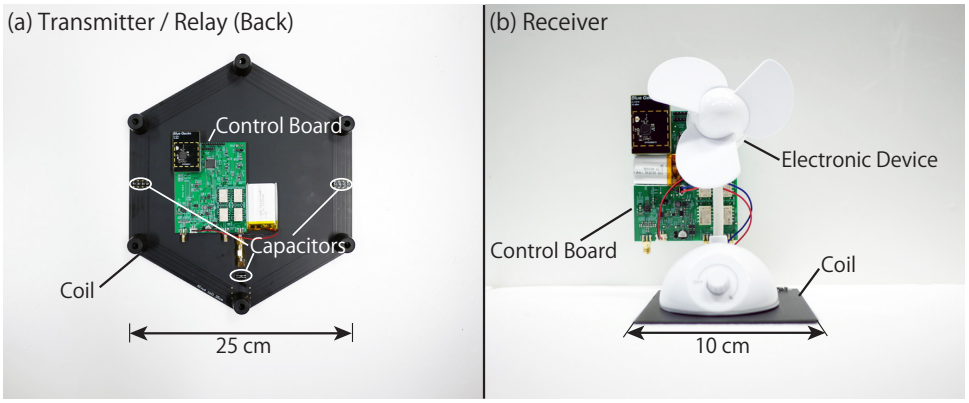

Fig. 7. Implemented resonator modules. Each module consists of a *LC* resonator (*i.e.*, coil and capacitor satisfying the series resonance condition [eq. (1)]) and a control board. (a) Transmitter and relay modules. (b) Receiver module. An electronic device connected to the control board is wirelessly charged.

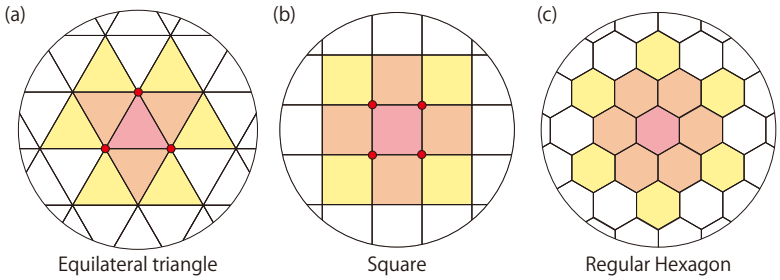

Fig. 8. Tiling patterns using convex regular polygons. There are only three convex regular polygons that can fill a plane: equilateral triangles, squares, and regular hexagons. In each figure, orange and yellow polygons represent the closest (*i.e.*, adjacent) and the second closest polygons to the red one, respectively. In the triangular tiling and the square tiling, there are points where the red polygon and the yellow polygons meet (red points shown in (a), (b)), whereas in the hexagonal tiling such points do not exist. Cross-coupling (in this figure, coupling between resonators on red and yellow tiles) must be avoided since it is known to degrade efficiency in multihop WPT. Therefore, we adopt hexagon as a shape of the resonator coil.

The next section focuses on the details of the implementation of these functions.

4 DESIGN AND IMPLEMENTATION

The implemented resonator module is shown in Fig. 7. Each module consists of a *LC* resonator (*i.e.*, coil made on PCB and lumped capacitor) and a control board, which can be configured to work as any type of resonator module (*i.e.*, transmitter, relay, and receiver) by switching a type-selector switch on the control board. This section first introduces the hardware implementation of Alvus, which enables the required functions mentioned in section 3.3. Then, the algorithm for the dynamic power routing mentioned in section 3.2.3 is described.

4.1 Resonator Coil

Hexagon coils were used for the transmitter and relay coil. The shape of transmitter/relay coil is required to be a regular polygon from the viewpoint of modularization; equilateral triangles, squares, regular hexagons are

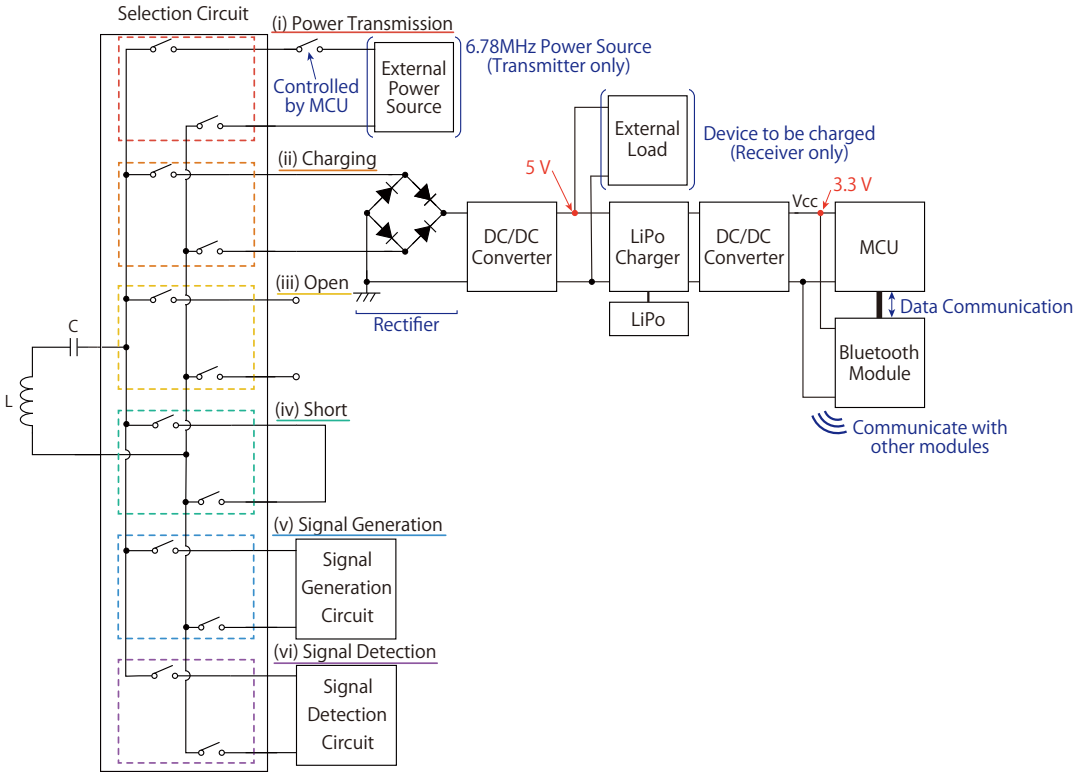

Fig. 9. Simplified circuit diagram of the Alvus resonator module. The selection circuit switches the connection to the *LC* resonator according to the intended resonator's operation mode.

the only regular polygons which can fill a plane. As mentioned in section 3.2.3, cross-coupling should to be avoided in multihop WPT, therefore it is beneficial that non-adjacent modules are positioned as far as possible. Consequently, regular hexagons are the best when taking this into consideration, as shown in Fig. 8.

Our system transmits power via multiple relay coils, so it is essential to minimize the loss at each relay coil. It is important to (a) increase the mutual inductance between transmitter/relay modules and (b) decrease the copper loss of each resonator (*i.e.*, use high Q-factor coils). Increasing the number of turns is a typical way to enhance mutual inductance; we also utilized "distributed reactance compensation (DRC)" technique [26] to suppress the electric field, which consequently decreases the dielectric loss. From the aforementioned requirements, we designed a 4-turn, 25 cm hexagon spiral coil; the resulting Q-factor was around 200 with the control board equipped. As for the receiver, a 6-turn, 10 cm × 10 cm square spiral coil with a Q-factor around 210 was used. Note that although we used fixed sized coils in this paper, the size/shape of these coils does not have to be the same, and can be freely designed based on the use-case.

4.2 Control Board

The functional diagram of the control board is shown in Fig. 9 and consists of the following:

- A microcontroller for controlling the module (STM32L073RZ)

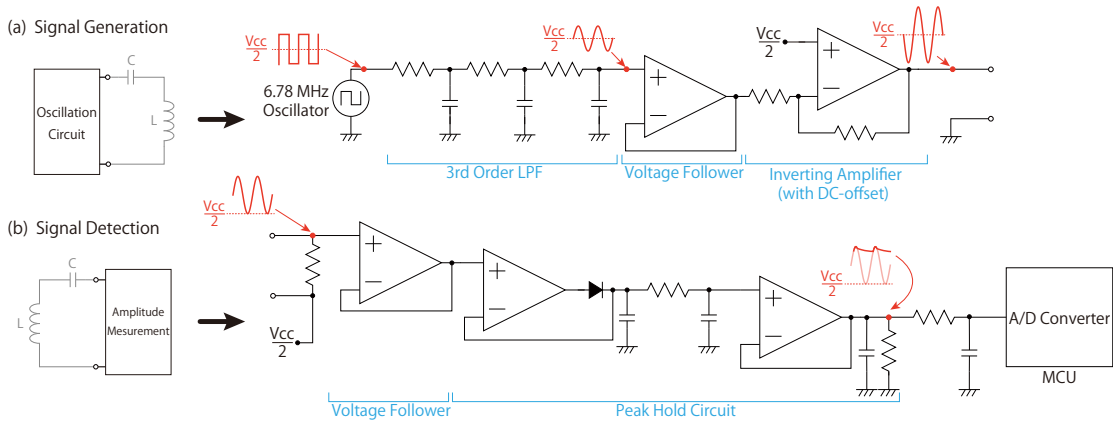

Fig. 10. Implementation of signal generation/detection circuit. (a) The signal generation circuit inputs a sine wave of 6.78 MHz into the *LC* resonator; consequently, a magnetic field oscillating at 6.78 MHz is generated. (b) The signal detection circuit acquires the amplitude of the sinusoidal voltage induced in the *LC* resonator by using the peak-hold circuit.

- Low-resistance mechanical relays for changing module state (TQ2SL-L2-3V-Z)
- High-frequency (6.78 MHz) signal generation/detection circuit
- Bluetooth mesh protocol communication modules (Silicon Labs EFR32BG13)
- A Li-Po battery used as an energy buffer for the control board on the module

The mechanical relays are controlled to switch between the six states shown in Fig. 9. The values of the mechanical relay's isolation and inserted loss at 6.78 MHz are approximately 65 dB and 0.05 dB, respectively[1]. This high isolation enables the relay to be completely isolated (*i.e.,* not function as a resonator) in open mode. The 6.78 MHz signal generation circuit was implemented as shown in Fig. 10 (a) and the signal detection circuit was implemented as shown in Fig. 10 (b). The signal generation circuit amplifies the signal generated by the 6.78 MHz crystal oscillator and inputs this signal to the resonator so that an oscillating magnetic field is generated. The signal detection circuit measures the intensity of this magnetic field through the voltage induced in the resonator. The induced voltage is converted to DC by a peak-detector and is input to an A/D converter on the microcontroller. Note that we cannot simply use the rectified receiver voltage as we need to set the input impedance of this detection circuit high to minimize the interference between multiple signal detection modules. Otherwise, current inevitably flows in the resonator connected the detection circuit, which affects the magnetic field distribution and consequently the read-out values of other detection mode modules.

As for the communication protocol, we used Bluetooth Mesh, which can establish a many-to-many (m:m) communication. In contrast to the ordinary Bluetooth method, where packets are delivered one-to-one, Bluetooth Mesh delivers packets from one module to all the modules through flooding. The Li-Po battery is an energy buffer used for powering the control board in both relay and receiver modules. As for the receiver module, this battery can also be configured so that it supplies power to an load (*i.e.*, target of power delivery) attached by the user. The microcontroller on each module monitors the voltage of the Li-Po battery; when this voltage falls below a

[1] https://www3.panasonic.biz/ac/e_download/control/relay/signal/catalog/mech_eng_tq.pdf

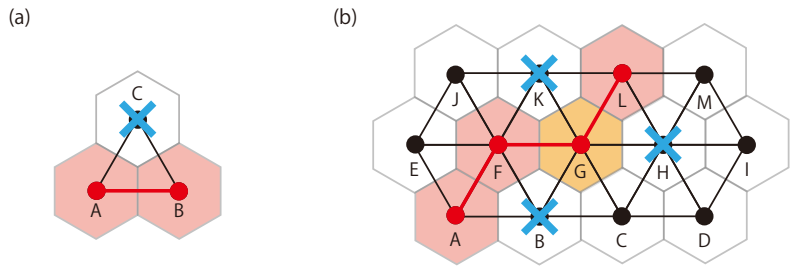

Fig. 11. Constraint to the power route that avoids cross-coupling. (a) When the red route (A–B) is established, cell C, which is adjacent to both A and B cannot be used; otherwise a cross-coupling occurs. (b) Assume that a red path (A–F–G–L) has already been established. When branching a new path from an orange cell G, cells with blue crosses (B, H, K) cannot be used. Cell C is the only module to proceed to from the cell G.

certain threshold, it sends out a request for power to the transmitter[2]. When this request is sent out, power is supplied from the transmitter to the relay in the same manner that the power is delivered to the receiver.

4.3 Dynamic Power Routing Algorithm

The pseudo code of the implemented routing algorithm is shown in Algorithm 1. When a power source (*i.e.*, transmitter), multiple destinations (*i.e.*, receivers), and a resonator map (*i.e.*, topology of the placement of transmitter/relay) are input to the algorithm, the routes are returned as an output.

Function FindRoute in the Algorithm 1 is a function that generates the route from the transmitter to a single receiver while avoiding cross-coupling. In the module map generation procedure, Alvus obtains the coupling between modules as a undirected graph; Alvus utilizes this graph to find available routes from the transmitter to the receivers. Now the route generation process can be abstracted to the process of determining a path between two nodes of the graph. Although there are many methods to determine a path between two nodes of graph, we chose to implement an algorithm based on the breadth-first search, since this generates the shorted path between the two nodes.

As shown in Fig. 11, not all nodes can be used since the established paths bring about constraints to avoid cross-coupling. By excluding these unavailable nodes, only routes without cross-coupling are explored; consequently, the solution space to be explored shrinks and the time used to search is shortened. Figure 12 describes the flow of the power route generation process; the function FindRoute is executed in an iterative manner until the routes that reach all receivers are determined. As mentioned in section 3.2.3, if foreign objects are detected by the route validation procedure, the system generates a route which avoids them; this is achieved by simply removing the module(s) on which the foreign object exists from the resonator map before the route calculation.

We note that whether all the receivers can be powered simultaneously via the abovementioned procedure depends on the configuration of the modules. Two example cases are shown in Fig. 13. In the case of Fig. 13(a), power can be supplied to all the receivers at the same time. However, if receivers are placed so that three cells are adjacent as shown in Fig. 13(b), cross-coupling occurs when we try to simultaneously charge all the receivers. This can be solved by introducing "time-division power supply". By alternately generating the routes shown by the red arrows and the ones shown by the blue arrows, it is possible to supply power to all the receivers without causing cross-coupling. In the current implementation, when a route that can simultaneously charge all

[2]Even in the case that the battery gets empty, our system can charge it. When the battery voltage falls below another threshold, relay modules automatically change its state to charge mode. Also, to ensure that "dead" relays are not missed, the transmitter periodically sends ACK packets to each relay to check if it is still active. In the case there is no response, the transmitter considers the relay to be dead and charges it.

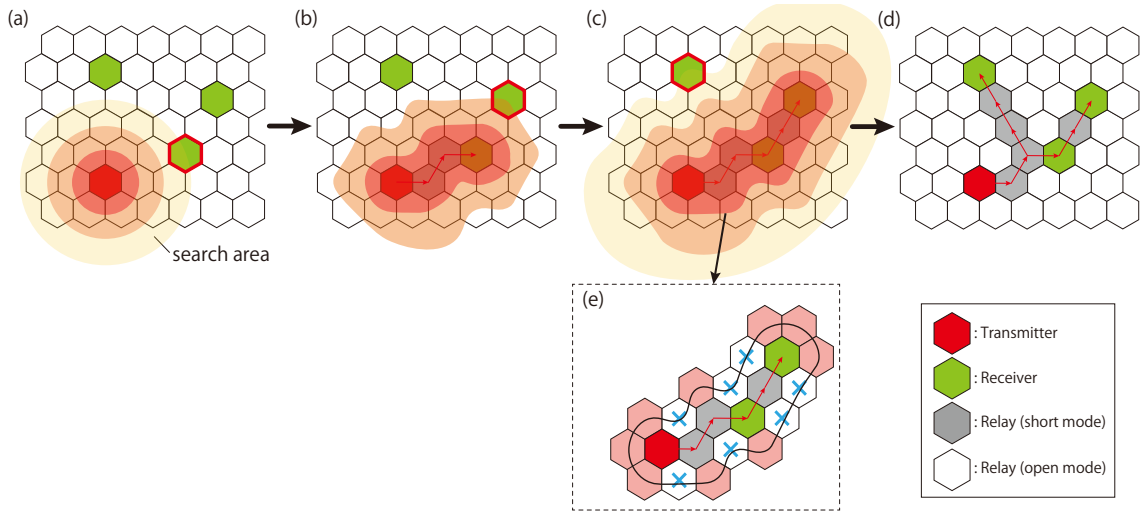

Fig. 12. Power route generation using breadth-first search (BFS). (a) Our algorithm finds the closest node from the transmitter. BFS finds the first receiver in three hops. (b) Next, our algorithm finds the next node, which is closest to the route generated in (a). (c) Similarly, subsequent nodes are routed in the same algorithm. The final route is shown in (d). Our algorithm reduces the candidate cells to be searched by applying constraints on cross-coupling. (e) This figure shows the actual candidates while searching the cells adjacent to the route in (c). The white cells with x are excluded from the search because they cause cross-coupling.

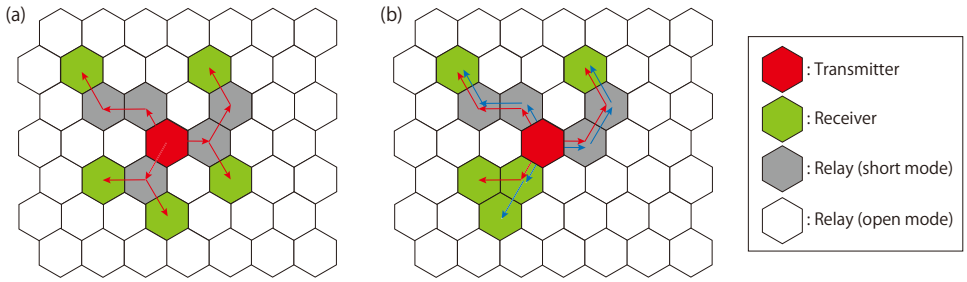

Fig. 13. Examples of the power route. (a) Example of power routes that can charge all receivers simultaneously. (b) Example of power routes that *cannot* charge all receivers simultaneously. In this case, a time-division power supply is required; the system needs to alternately generate the red routes and the blue routes.

the receivers (let n be the number of the receivers) at once cannot be found, the routing algorithm outputs n routes that reach each receiver via the shortest path; these routes are configured one a time so that each receiver can receive power in turn.

5 EVALUATION

5.1 Power Transfer Efficiency

In this section, we evaluate the power transfer efficiency of Alvus through measurements. Since Alvus delivers power using multihop WPT, copper loss occurs in each relay coil on the route. Therefore, one interest is the

ALGORITHM 1: Generating routes from the transmitter to the receivers

```
Procedure RouteGeneration :
    input  : Transmitter node Source, List of receiver nodes Destinations, Resonator map M
    output : List of routes Routes
    n ← the number of destinations;
    Routes ← new List;
    for i ← 1 to n do
        Destination ← i-th element of Destinations;
        Route ← FindRoute(Source, Destination, M, Routes, i);      ▹search for a route for i-th destination
        if route was found then
            append Route to Routes;
        else
            if i = 1 then
                return time-division routes;      ▹there are no routes that can simultaneously charge all receivers
            else
                i ← i − 1;                        ▹revert to the search for the previous destination
            end
        end
    end
    return Routes;                                ▹return the generated routes
end

Function FindRoute :
    input  : Transmitter node Source, Receiver node Destination, Resonator map M, Established routes Routes, Index of
             destination i
    output : Route from the transmitter to the receiver Route
    if this is the first search for the i-th route then
        Q ← new Queue;
        foreach module m in Routes do
            enqueue m into Q;                     ▹append the modules on the routes to the search candidates
        end
    else
        restore Q to the last state of the i-th search;   ▹continue to search from where we ended last time
    end
    while Q is not empty do
        target ← dequeue from Q;
        adjacent_modules ← enumerate all modules adjacent to target using a resonator map M;
        foreach module_to_be_searched in adjacent_modules do
            if module_to_be_searched is Destination then          ▹if a route was found, return it
                return the route from Source to Destination
            else if module_to_be_searched is available then       ▹if the module will not cause cross-coupling,
                enqueue module_to_be_searched to Q                ▹append the module to the search candidates
            end
        end
    end
    return empty route;                           ▹there is no route to the destination
end
```

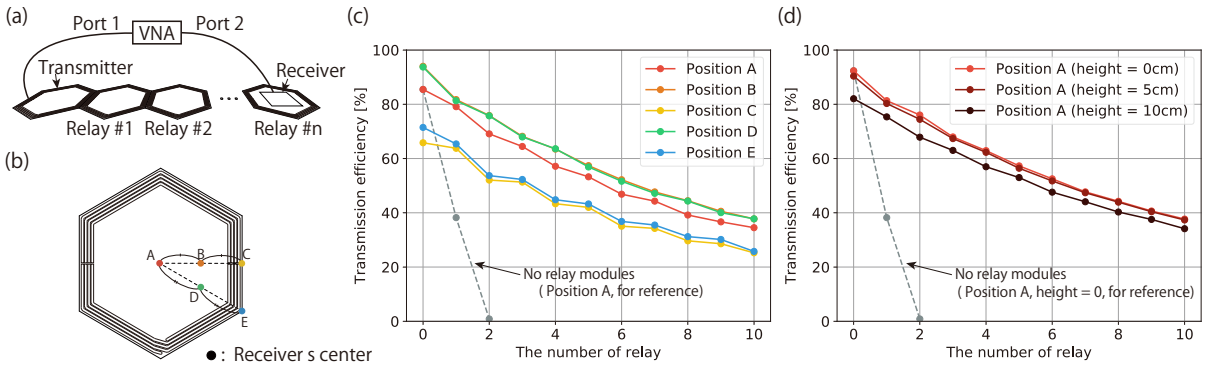

Fig. 14. Evaluation of the power transfer efficiency. The dotted lines in (c) and (d) represent situations where the power is directly delivered from the transmitter to the receiver without any relay module, as shown in Fig. 2(a); this corresponds to the situation where all the relay modules are removed in the measurement of the efficiency of red line (*i.e.*, Position A).

relationship between the number of "hops" and efficiency. As we consider 2-D WPT systems, our system needs to be robust against parallel misalignment, therefore we also conducted the "number of hops" measurement under the condition that the receivers are misaligned. Another interest we consider is whether the efficiency is dependent on the shape of the route when the number of hops is a fixed number. Furthermore, we evaluate the loss of efficiency caused by cross-coupling and see if this drop can be avoided by using an alternative route. Finally, the DC-to-DC power transfer efficiency, that is, end-to-end power transfer efficiency of our system is evaluated.

5.1.1 The Number of Hops and Misalignment of Receiver. The measurement setup is shown in Fig. 14(a). A vector network analyzer (VNA) is used to extract the S-parameters from the transmitter to the receiver. Note that n relay modules are linearly arranged between the transmitter/receiver pair without physical connection. The receiver module is placed on the n-th relay (or the transmitter when $n = 0$) and power is transferred via $n + 1$ hops. Using the measured S-parameters, we calculated the maximum transfer efficiency when the real part of load impedance can be varied [28]. We used this figure of merit since it is known that the real part of load impedance can be adjusted through the voltage conversion ratio of DC/DC converters, whereas the tuning of the imaginary part of load impedance is still an challenge unless bulky capacitor banks are used. This calculated value was used as measured efficiency. As our focus is not to optimize impedance conversion mechanisms but to provide a proof of concept of a reconfigureable 2-D WPT system, we consider the integration of these maximum efficiency point tracking mechanisms as future work.

The measured efficiencies when the receiver module is placed on the five points shown in Fig. 14(b) are shown in Fig. 14(c); this is the power transfer efficiency with n relays and lateral misalignment. The efficiency with the relay coils removed are also plotted for reference [the Fig. 2(a) case]. It can be seen that positions A, B, and D show nearly the same efficiency, whereas C and E show a 10% to 20% drop, although the efficiency exceeds 40% efficiency in a large area.

The next factor we considered is vertical misalignment. We aligned the n-th relay coil and the receiver coil and set the height of the receiver to $h = 0, 5, 10$ cm. We note that 10 cm is equal to the length of one side of the receiver's coil [see Fig. 7]. The results are shown in Fig. 14(d). We can see that the degradation of efficiency when the distance is extended from 0 cm to 10 cm is around 10% at most. This confirms that Alvus is capable of scenarios where the transmitter/receiver are separated, such as when placing relay modules under the table and the powering devices on the table.

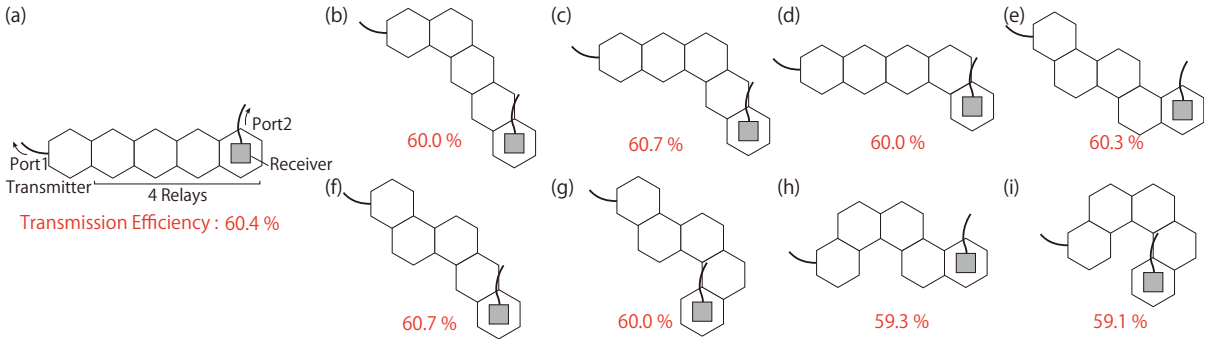

Fig. 15. Evaluation of the power transmission efficiency when a power route is bent. The efficiency of the bent routes [(b)–(i) in the figure] are approximately equal to that of the straight route [(a) in the figure].

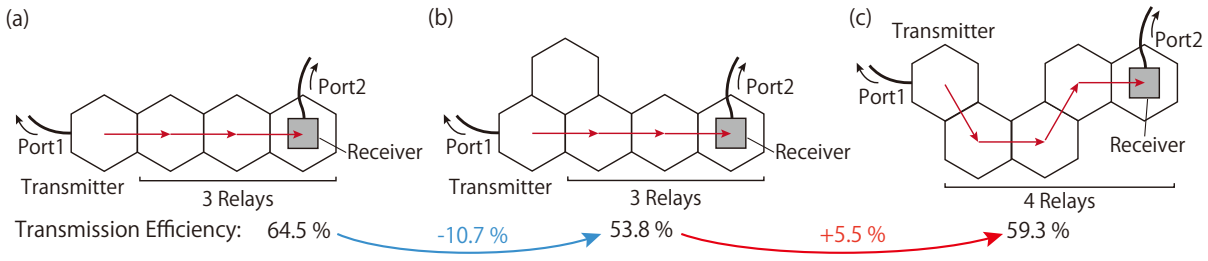

Fig. 16. Evaluation of the efficiency degradation caused by cross-coupling. (a) A straight 4-hop power transmission route. (b) A relay module (short mode) added so that it causes cross-coupling. The cross-coupling degrades the power transmission efficiency by 10.7%. (c) Avoiding the cross-coupling by taking a detour. The efficiency increased by 5.5% over (b).

From Fig. 14(c)(d), we notice that even when power is delivered via 10 relay modules, the transmission efficiency keeps a value around 30% to 40%. Since the width of the transmitter and the relay coils are 25 cm [see Fig. 7(a)], the length of 10 relays is 2.5 m. Consequently, Alvus can cover the area of 5 m diameter (*i.e.*, approximately 19.6 m^2) by placing untethered relay modules around the transmitter.

5.1.2 Bending the Power Route. Next, we investigated the variation of the power transmission efficiency when the power route is bent. One transmitter and four relays are arranged so that cross-coupling does not occur, and the receiver is placed on the center of the fourth relay module. The transmission efficiency was measured in the same manner as in section 5.1.1. The evaluated routes and the corresponding efficiencies are shown in Fig. 15. We can see the efficiencies of the bent routes are approximately equal to those of the straight route; this means that the efficiency is nearly independent to the geometry as long as the number of hops are the same and cross-coupling does not occur.

5.1.3 Cross-Coupling. Next, we evaluated the efficiency degradation caused by cross-coupling. As shown in Fig. 16(a), the transmission efficiency using a straight 4 hop power route is 64.5%. Fig. 16(b) shows that when a new relay module is placed so that it causes cross-coupling (this corresponds to situations such as when the branch of the power route appears), the efficiency drops by 10.7%. Furthermore, in Fig. 16(c), it is shown that Alvus can mitigate this efficiency drop by taking a detour. Although an additional loss of a few percent is induced by the extra one hop, the resulting efficiency increases by 5.5% when compared to the cross-coupled case.

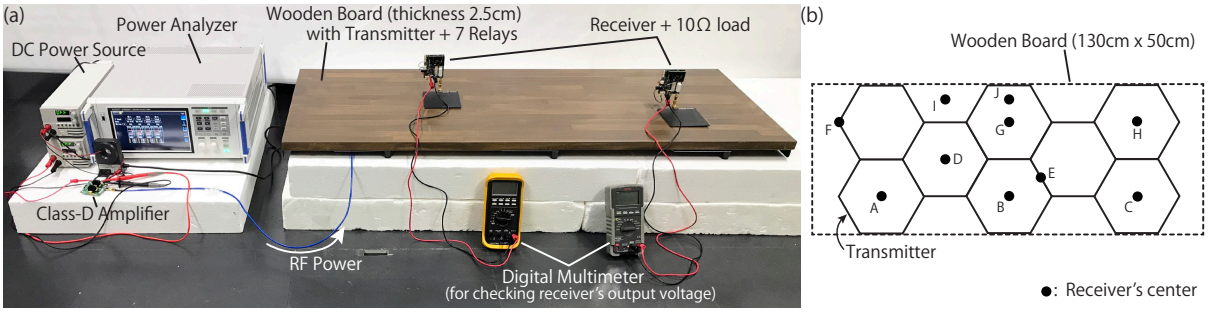

Fig. 17. Evaluation of the DC-to-DC power transfer efficiency. (a) Experimental setup. (b) Placement of resonator modules and positions where the receivers were placed.

Table 1. DC-to-DC power transmission efficiency.

(a) single receiver

Receiver	Input power	DC-to-DC efficiency	Overall efficiency
A	5.24 W	53.1%	46.7%
D	6.42 W	43.4%	39.0%
E	8.36 W	33.3%	30.7%
F	8.92 W	31.1%	28.8%
H	8.38 W	33.2%	30.6%
I	10.76 W	25.9%	24.2%
J	6.71 W	41.5%	37.5%

(b) two receivers

Receiver #1	Receiver #2	Input power	DC-to-DC efficiency	Overall efficiency
A	B	13.57 W	40.6%	38.5%
A	E	16.19 W	34.2%	32.8%
A	G	13.47 W	41.0%	38.9%
D	B	12.70 W	43.5%	41.2%
D	C	14.65 W	37.7%	35.9%

5.1.4 DC-to-DC Power Transfer Efficiency. Finally, we evaluated the end-to-end power transmission efficiency of our system, assuming the scenario of creating a wireless charging shelf[3] using Alvus. We taped Alvus modules (one transmitter and seven relays) to the back of a wooden board (width: 130 cm, depth: 50 cm, thickness: 2.5 cm) as shown in Fig. 17(a).

RF current was input to the transmitter module via a class-D amplifier powered by a DC power source, and the receiver was loaded with a 10 Ω resistor, premising the voltage/current ratio of a typical USB2.0 (5 V, 0.5 A) charger. The transferred RF power was rectified via a full-bridge rectifier, regulated via a buck-converter, and then input to the 10 Ω load. The DC-to-DC efficiency was evaluated by measuring the input DC power and the DC power consumption at the load. Since the transfer efficiency depends on the DC voltage powering the class-D

[3]This is also demonstrated as an application in section 6.1.1.

amplifier, we manually swept the input voltage and measured the value when the efficiency was maximized [28]. Although our current implementation of Alvus does not automate this sweeping function, it can be integrated by adding monitoring circuits for input voltage/current and using programmable power sources [see section 6.2.1]. Also, note that the constant parameter in this evaluation is transferred power. Since the receiver is connected to a voltage regulator and the load is a resistor, the power consumed at the load is constant and the input power varies depending on the DC-to-DC efficiency. We also evaluated the overall power efficiency considering the power consumption overhead of all modules composing the array. Since it was difficult to directly measure the power consumption of all modules at once, we added "the power consumption of relay resonators [see section 5.5]" to the "input power" and treated it as the overall power consumption. Note that the overall efficiency will approach the DC-to-DC efficiency asymptotically as (i) the transferred power gets larger or (ii) the power consumption of each module gets smaller.

First, we evaluated the efficiency when a single receiver is placed on the positions shown in Fig.17(b). The efficiency at each position is shown in Table 1(a). We can see that the efficiency decreases as the distance from the transmitter (*e.g.*, number of hops) increases. From the results at position F and I, we observe that the power supply range is not strictly limited to the surface of the modules but also covers the proximity of the modules. We note that there is a non-negligible decrease in efficiency when compared to AC-to-AC evaluations in sections 5.1.1 and 5.1.2. This is due to the losses in DC/AC, AC/DC, and DC/DC conversions. By improving the conversion efficiency, the gap between AC-to-AC and DC-to-DC efficiencies can be mitigated; we consider this optimization out-of-scope.

Next, we measured the efficiency when two receivers are charged simultaneously. The results are shown in Table 1(b). These results confirm that Alvus is capable of delivering several watts to multiple devices simultaneously. We also observe a fluctuation in efficiency when the positions of the receivers are varied. Our route generation method does not guarantee maximum efficiency to all devices when there are multiple devices; this limitation is discussed in section 6.2.1.

5.2 Resonator Detection

Next, we evaluated the performance of resonator detection (*i.e.*, relay detection and receiver proximity detection). Both the detection of relays and receivers utilize the same mechanism shown in Fig. 4. The measured value varies by the resonator position (*i.e.*, mutual inductance between two resonators). Therefore in this section, we investigated if this variation is sufficient to (i) detect adjacent coils among non-adjacent coils and (ii) localize the receiver.

5.2.1 Relay Detection. First, we evaluated the voltage induced in the signal detection mode module when the distance between the two relay modules is varied. The purpose of relay detection is to acquire the adjacent resonator, so a certain resonator ("Target" relay shown in Fig. 18) should be detected as adjacent only by the adjacent resonators (*i.e.*, "relay A"s in Fig. 18). In other words, there should be a sufficient difference between the measured voltage on the resonators A and the voltage on the resonators B, C shown in Fig. 18(a). In order to verify this, we evaluated the relationship between the distance between the centers of the two relay modules (parameter d shown in Fig. 18(b)) and the voltage measured by the resonator modules ($|V_2|$ in Fig. 4(a)). This measurement was conducted by using two resonator modules: one in signal generation mode and one in signal detection mode. The result is shown in Fig. 18(c). The distance d was changed in intervals of 5 cm, and two ways of coil placement were considered [see Fig. 18(b)]. Also, we note that the plotted value is the average of 100 measured values. The voltage values measured at the position of the resonator A, B, C are 2991 mV, 1777 mV, 1715 mV, respectively. Since there is a large difference between the value acquired at the position of resonator A and that of B and C, we confirm that resonators can detect the adjacent modules by setting an appropriate threshold.

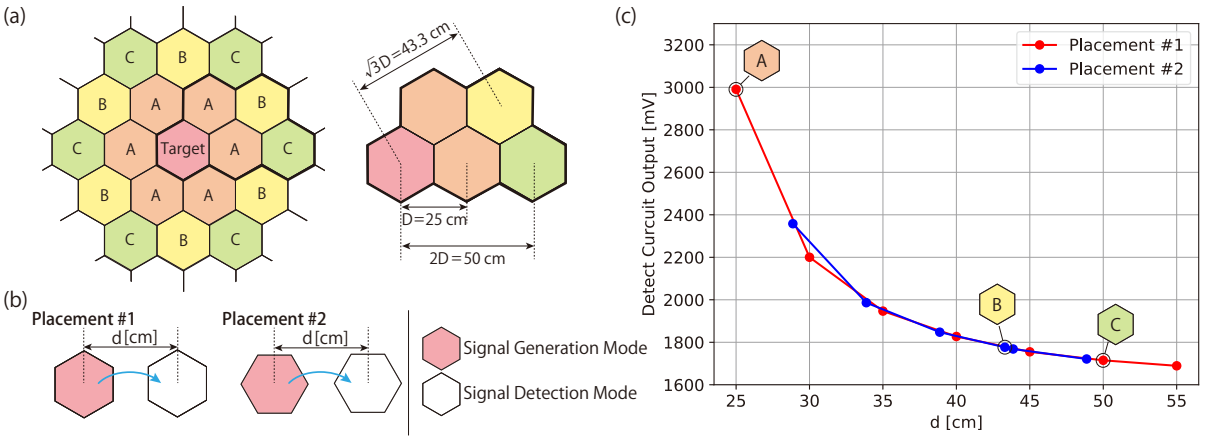

Fig. 18. Evaluation of the relay detection performance.

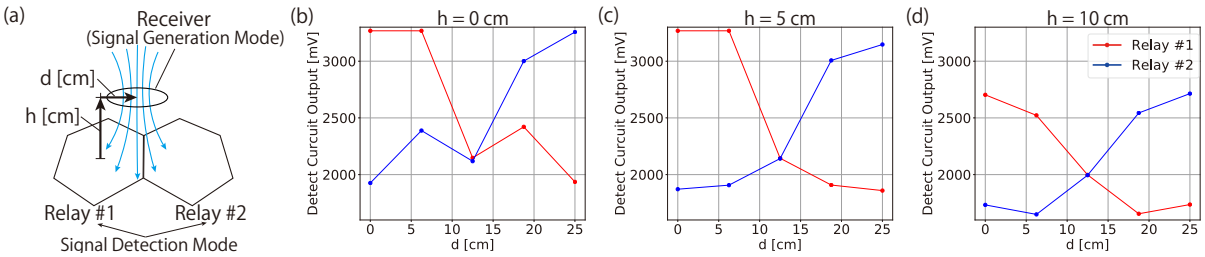

Fig. 19. Evaluation of the receiver proximity detection performance.

5.2.2 Receiver Detection. Next, we evaluated the voltage induced in the signal detection mode module with various receiver positions. The receiver generates an oscillating magnetic field, whereas the transmitter/relay modules measure the signal amplitude; this mechanism is used for the receiver proximity detection process before power routing. The requirement of this function is that each transmitter/relay module can estimate how close (*i.e.*, strongly coupled) the receiver is to itself, and be able to easily distinguish the closest transmitter/relay module. The measurement was conducted as shown in Fig. 19(a); the receiver generates a 6.78 MHz magnetic field whereas the voltage induced on two relay modules were measured. The receiver was placed on the six points ($d = 0, 5, 10, 15, 20, 25$ cm), with three heights ($h = 0, 5, 10$ cm) and the output of the detection circuit for each case is shown in Fig. 19(b)–(d). It can be seen that the mechanism has a sufficiently large dynamic range, therefore, the closest (*i.e.*, the most strongly coupled) transmitter/relay module can be easily estimated through Eq. 3. Note that it is necessary to know the closeness in terms of magnetic coupling, therefore even in the case that the detection values do not directly collate with physical distance [see Fig. 19(b), Relay #1 case where we can see a local maximum around $d = 20$].

5.3 Foreign Object Detection

To evaluate the foreign object detection function, we placed various metallic objects which are likely to be placed on everyday surfaces and investigated how they affect the system. The objects we considered are shown in Fig. 20(b)–(e): (b) coins, (c) paper clips, (d) key-chains, and (e) metallic toolbox; we also placed (a) open

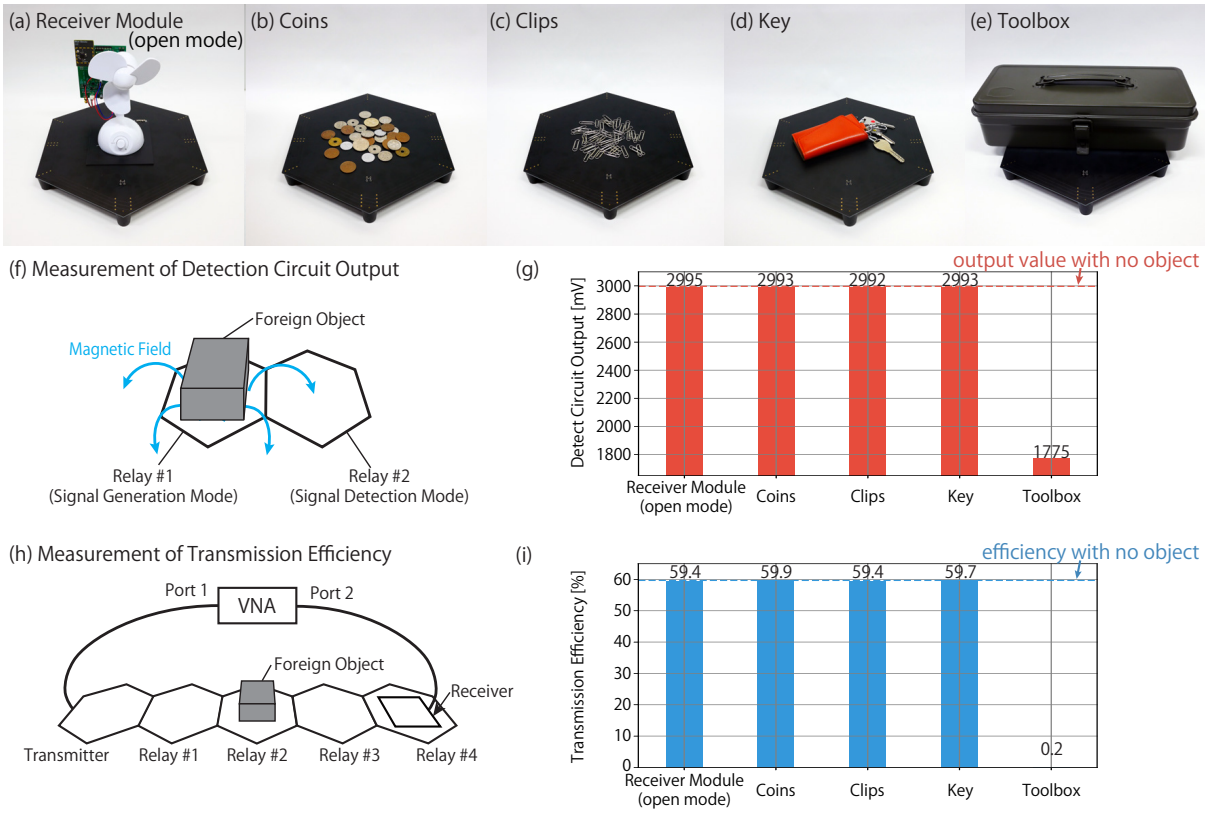

Fig. 20. Evaluation of the foreign object detection performance. (a)–(e) Objects we used for the evaluation. (f),(g) Measurement of output value of the detection circuit. (h),(i) Measurement of the power transfer efficiency.

mode (*i.e.*, off state) receivers to see if this interferes with the system. For this evaluation, we first conducted the object detection function, which is basically the same as the map generation function but only performed on the modules on the route, and examined if the induced voltage is affected by objects; if the fluctuation of the induced voltage can be observed by the signal detection circuit, these objects can be detected. The measurement procedure is shown in Fig. 20(f). After this observation, we measured the transfer efficiency in the case that these objects exist on the power route, as shown in Fig. 20(h). The results are shown in Fig. 20(g),(i). The dotted lines show the values with no foreign object placed. It can be seen that the case for which efficiency significantly degrades corresponds with the case for which the detected value drops; Alvus's foreign object detection function can detect objects that significantly degrade efficiency in advance. Using this information, our system can construct a route that takes a detour around these obstructive objects. We note that our considerations in this study are envisioning up to a few Watts of power transfer, therefore we consider that only accounting for loss of efficiency is enough. In high-power systems (*e.g.*, kilowatts) some reports show that even a small portion of energy used to heat up coils can lead to danger. Although the current system of Alvus does not account for this, we note that further consideration should be made when attempting high-power transmission for higher magnitudes. It is also shown from the Fig. 20(a) case that the receiver module in open mode does not affect either the detection

Table 2. Time consumption of each step.

Step	Transmitter + 5 Relays				Transmitter + 7 Relays			
	time [ms]	comm. [%]	meas. [%]	proc. [%]	time [ms]	comm. [%]	meas. [%]	proc. [%]
Map Generation	7465	98.2	1.2	0.6	9616	98.2	1.1	0.6
Rx Detection	1139	96.8	2.6	0.6	1136	96.7	2.6	0.6
Route Calculation	11	0.0	0.0	100.0	24	0.0	0.0	100.0
Foreign Obj. Det.	2592	97.8	1.9	0.4	2592	97.8	1.9	0.4
Start Powering	148	91.9	0.0	8.1	148	91.9	0.0	8.1

Note: The values of the column of "comm.", "meas.", and "proc." represent the percentages of the time spent on communication, measurement, and processing, respectively.

Table 3. Power consumption of resonator module.

	Open mode	Short mode	Signal generation mode	Signal detection mode	
				w/input signal	w/o input signal
$V_{\mathrm{LiPo}} = 4.2\,\mathrm{V}$	90.3 mW	90.3 mW	314.6 mW	276.7 mW	252.4 mW
$V_{\mathrm{LiPo}} = 4.0\,\mathrm{V}$	86.8 mW	86.3 mW	310.8 mW	273.6 mW	248.4 mW
$V_{\mathrm{LiPo}} = 3.7\,\mathrm{V}$	81.4 mW	81.4 mW	308.2 mW	270.8 mW	244.9 mW

Note: "input signal" represents the oscillating magnetic field generated by an adjacent module in the signal generation mode.

voltage or the transfer efficiency; this means that the off-state receivers can be successfully decoupled (*i.e.*, made invisible) from the system, which allows flexibility in system operation.

5.4 Latency

Next, we evaluated the time consumed in each stage of operation: (1) resonator map generation, (2) receiver proximity detection, (3) dynamic power routing, and (4) powering each module. The dynamic power routing function consists of two sub-stages (*i.e.*, route calculation and route validation), so we evaluated them separately. To observe the effect caused by the increase in the number of modules, we conducted the test premising two configurations: (a) one transmitter and five relays, and (b) one transmitter and seven relays.

The results are shown in Table 2. In addition to the time consumption at each stage, we also measured the breakdown (*i.e.*, time used for communication, measurement, and processing) in each stage. Results show that the most remarkable cause of delay is communication, which will consequently loom as a bottleneck when charging quickly moving receivers; this limitation is discussed in section 6.2.2.

5.5 Power Consumption

Finally, we evaluated the power overhead of the modules. The relay module operates in four modes: open mode, short mode, signal generation mode, and signal detection mode. We evaluated the power consumption of each mode by substituting the LiPo battery with a source meter. The results are shown in Table 3. The open mode and short mode consumed the same amount of power of around 90 mW. The signal generation/detection mode consumed power of at most 315 mW and 280 mW, respectively. Although this power consumption is not small, the time corresponding to this mode is considerably short compared to other components as shown in the “meas.”

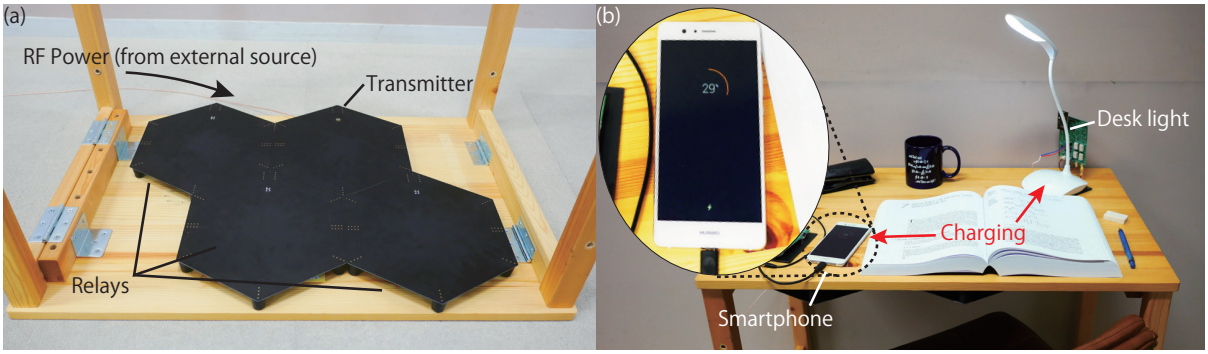

Fig. 21. Demonstration of a wireless charging desk. By just laying Alvus modules on the back of the desk, we can transform a regular desk into a wireless charging desk.

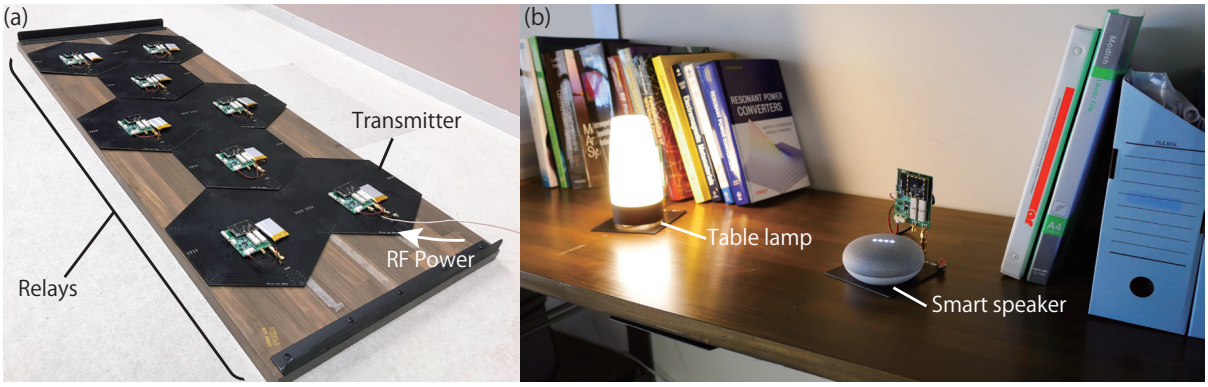

Fig. 22. Demonstration of a wireless charging shelf. The table lamp and the smart speaker are powered wirelessly.

column in Table 2; therefore, we roughly approximated that the total power consumption of the module averaged over time is around 90 mW.

6 DISCUSSION

6.1 Applications

Potential applications of Alvus widely range from personal to industrial use-cases. For example, users can add wireless charging capabilities to ready-made furniture simply by placing tiles on it, or even transform whole factory floors into WPT surfaces to empower industrial robots. We demonstrate the capabilities of our prototype through three scenarios: a wireless charging desk, a wireless charging shelf, and a wirelessly powered robot.

6.1.1 Wireless Charging Furniture. Many electronics are placed on furniture. For example, many desks are equipped with desk lights, monitors, etc. Moreover, many mobile electronics such as smartphones and laptop computers are occasionally charged on desks as people stop by. Supplying power to these devices through cords not only limits mobility but also causes messy workplaces. WPT technology allows users to charge devices by simply placing them on the surface; this can make charging activities "unconscious". Today's wireless charging

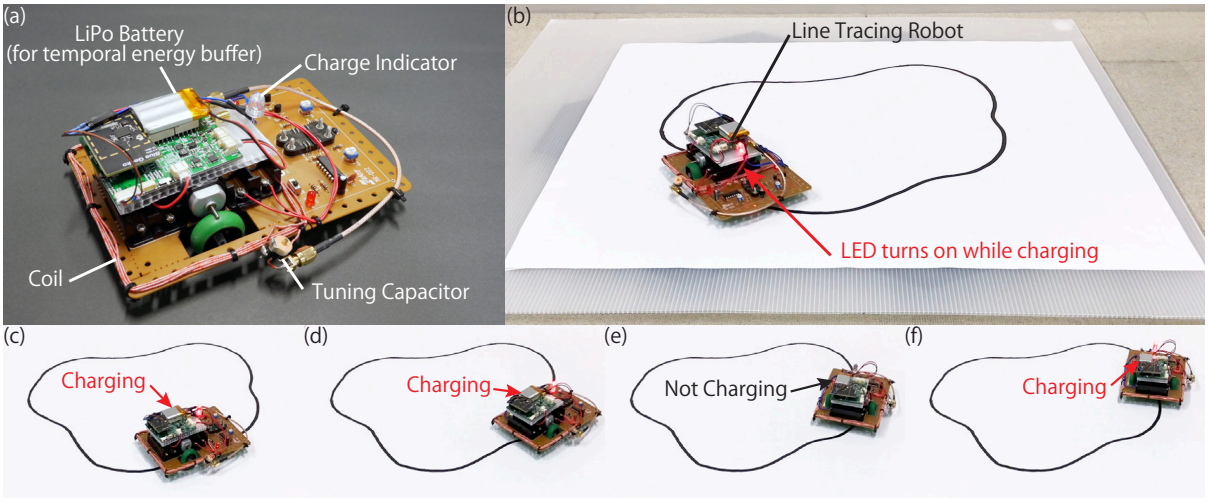

Fig. 23. Demonstration of a wirelessly powered robot. The LiPo battery installed in the line tracing robot is charged wirelessly. Since the system detects the position of the robot and re-generates the power supply path toward the new position, Alvus can also be applied to moving objects.

technology realizes manufacturing order-made desks with wireless charging capabilities integrated. However, manufacturing these desks would be extremely expensive.

We show in Fig. 21(a) that we can retrofit typical, ready-made desks into wireless charging desks, simply by taping Alvus modules to the back of the top board. When electronics equipped with Alvus's receiver modules are placed on the desk, Alvus automatically detects the devices, constructs a route, and charges them as demonstrated in Fig. 21(b).

Similarly, we demonstrated that the same concept can be easily modified to fit shelves as shown in Fig. 22. By taking off the modules on the desk, re-arranging them to fit on shelf boards, and taping them to typical, ready-made shelves, these shelves can be instantly transformed into charging cabinets, where stowed electronics can be charged in a seamless manner.

6.1.2 Wirelessly Powered Robots. Alvus can also potentially work as a means of supplying energy to moving robots. Due to the autonomous and mobile nature of robots, seamless power supply is desired for continuous operation of the robots. Nowadays, power supply to the robots is realized by charging cradles, manual charging, or equipping large batteries, but these methods are likely to scale-out (*e.g.*, many obstructive charging cradles, huge batteries, etc); turning the floor into a wireless charger is an option, although this requires a huge cost for construction/renovation.

Alvus can solve this problem by retrofitting typical floors into wireless charging surfaces. To show a functional prototype, we arranged Alvus modules on the floor like carpet tiles and charged a line tracing robot as shown in Fig. 23. While the robot moves around the surface, Alvus dynamically detects the module closest to the robot, re-constructs the power route, and wirelessly charges the battery connected to Alvus's receiver module; this battery works as a buffer and enables the robot to move continuously. Since in our current implementation, the receiver detection and power supply cannot be performed simultaneously, a "dead-time", the time period that the robot is not charged, exists; however, as soon as the system re-locates the receiver, Alvus establishes the new power route and resumes charging [see Fig. 23(c)–(f)].

We note that we conducted this demonstration with the route validation function (*i.e.*, foreign object detection) disabled so as to reduce the overhead. This is certainly a limitation, although the main cause is the delay of communication as mentioned in section 5.4. Operation with all functions activated can be achieved by optimizing the communication protocol, which is a potential future research direction.

6.2 Limitations and Future Works

6.2.1 Power Transfer Efficiency. The factors that underlies in efficiency enhancement for general WPT systems are multi-fold, however in on our Alvus concept, there are two core factors that need to be considered: (a) maximum efficiency point tracking and (b) optimum route generation. As for (a) in "single" receiver cases, methods and implementations found in previous literature can be easily applied [28]. These studies can also be naively applied to "multiple" receiver systems by applying time-division multiplexing and charging each receiver one by one. Ideally, in this case, there is no upper limit for the number of receivers. However, each receiver experiences periodical "dead-times" when devices are not charged. To avoid this, the system can also generate routes to direct power to multiple receivers simultaneously. However, the extremely complex analytic formulation in this case makes it difficult to discuss the theoretical maximum efficiency conditions; therefore we leave this for future work.

6.2.2 System Overhead. Minimizing the system overhead is another important direction for future work; this was revealed as a limitation when demonstrating the wireless charging of moving robots [see section 6.1.2]. As discussed in section 5.4, the most significant cause of overhead in Alvus is the time delay of the messages, which is restricted by the communication protocol (Bluetooth Mesh in current implementation). Optimizing communication protocols or using other out-of-bound communication channels should be an effective approach to speed-up operations such as route construction and receiver detection.

Another fundamental cause of overhead derives from the system operation procedure; the current implementation cannot execute the power supply and detection procedures (resonator map generation, receiver proximity detection, and foreign object detection) at the same time; therefore the time for detection inevitably becomes "dead times" for charging. This dead time impacts system performance in the following situations: (1) when one receiver is moved while the other receivers should be kept charged continuously, or (2) when charging moving devices (*e.g.*, wirelessly charged robots). One promising solution is to use different frequency bands for charging and detection mechanisms (*i.e.*, frequency-domain multiplexing), instead of the current implementation which is based on time-domain multiplexing.

6.2.3 Interference of Surface Material (Coupling with the Ground). For the sake of simplicity, we did not consider the interference of surface material in this study. Through building applications, it was shown that our prototype works well when taped on wooden furniture or placed on the floor, therefore we considered that the effect of surface material is a minor issue in these cases. We note that when placing the device on the floor, rubber legs of 24 mm in height were attached on the back of the modules to accommodate the control board and battery between the coil and the floor. Considering a hypothetical case where the surface is composed of conductive material (*e.g.*, aluminum, copper, iron, etc), eddy current will occur on the surface, which will induce copper loss as well as frequency shifts and significantly affect system performance. We will investigate these effects and explore methods to isolate surface material and Alvus modules (*e.g.*, shielding with ferrite material) in the future.

6.2.4 Miniaturization/Optimization of Control Board. In the current implementation, the footprint and power consumption are not optimized because there are various functions left for debugging and further development. By fabricating custom designed integrated circuits (IC), it would be possible to reduce the size and the power consumption.

7 CONCLUSION

In this paper, we presented Alvus, a reconfigurable wireless charging system that enables the construction of wireless charging surfaces by simply laying ready-made modules. Alvus can retrofit everyday surfaces (desks, shelves, floor, etc.) into wireless charging surfaces in an instant and interactive manner. We discussed the design requirements, implemented a hardware prototype, evaluated the system performance, and provided potential applications of Alvus. Through the measurements, it was shown that Alvus can charge devices within a 19.6 m^2 area with an efficiency of over 25%.

ACKNOWLEDGMENTS

We thank Atsushi Sasaki and Arata Hashizume for their help on hardware design. We also thank Takashi Ikeuchi and Koya Narumi for their help in video shooting. This work was supported by JST ERATO under Grant No. JPMJER1501, Japan, and Grand-in-Aid for JSPS Fellows under Grant No. JP18J22537, Japan.

REFERENCES

[1] Juan M. Arteaga, Samer Aldhaher, George Kkelis, Cristopher Kwan, David C. Yates, and Paul D. Mitcheson. 2018. Dynamic Capabilities of Multi-MHz Inductive Power Transfer Systems Demonstrated with Batteryless Drones. *IEEE Transactions on Power Electronics* (2018), 1–1. https://doi.org/10.1109/TPEL.2018.2871188

[2] Suzhi Bi, Chin Keong Ho, and Rui Zhang. 2015. Wireless powered communication: Opportunities and challenges. *IEEE Communications Magazine* 53, 4 (April 2015), 117–125. https://doi.org/10.1109/MCOM.2015.7081084

[3] William C Brown. 1984. The history of power transmission by radio waves. *IEEE Transactions on Microwave Theory and Techniques* 32, 9 (September 1984), 1230–1242. https://doi.org/10.1109/TMTT.1984.1132833

[4] Matthew J Chabalko, Mohsen Shahmohammadi, and Alanson P Sample. 2017. Quasistatic Cavity Resonance for Ubiquitous Wireless Power Transfer. *PloS ONE* 12, 2 (February 2017), e0169045. https://doi.org/10.1371/journal.pone.0169045

[5] Andreas Christ, Mark G Douglas, John M Roman, Emily B Cooper, Alanson P Sample, Benjamin H Waters, Joshua R Smith, and Niels Kuster. 2013. Evaluation of wireless resonant power transfer systems with human electromagnetic exposure limits. *IEEE Transactions on Electromagnetic compatibility* 55, 2 (April 2013), 265–274. https://doi.org/10.1109/TEMC.2012.2219870

[6] Xiaoran Fan, Han Ding, Sugang Li, Michael Sanzari, Yanyong Zhang, Wade Trappe, Zhu Han, and Richard E. Howard. 2018. Energy-Ball: Wireless Power Transfer for Batteryless Internet of Things Through Distributed Beamforming. *Proc. ACM Interact. Mob. Wearable Ubiquitous Technol.* 2, 2, Article 65 (July 2018), 22 pages. https://doi.org/10.1145/3214268

[7] Arata Hashizume, Yoshiaki Narusue, Yoshihiro Kawahara, and Tohru Asami. 2017. Receiver localization for a wireless power transfer system with a 2D relay resonator array. In *2017 IEEE International Conference on Computational Electromagnetics (ICCEM)*. 127–129. https://doi.org/10.1109/COMPEM.2017.7912817

[8] Shu Yuen Ron Hui, Wenxing Zhong, and Chi Kwan Lee. 2014. A critical review of recent progress in mid-range wireless power transfer. *IEEE Transactions on Power Electronics* 29, 9 (September 2014), 4500–4511. https://doi.org/10.1109/TPEL.2013.2249670

[9] Airfuel Inc. 2018 (accessed August 15, 2018). *AirFuel Alliance*. https://www.airfuel.org/about/.

[10] Hamid Jabbar, Young S Song, and Taikyeong Ted Jeong. 2010. RF energy harvesting system and circuits for charging of mobile devices. *IEEE Transactions on Consumer Electronics* 56, 1 (February 2010), 247–253. https://doi.org/10.1109/TCE.2010.5439152

[11] Jouya Jadidian and Dina Katabi. 2014. Magnetic MIMO: How to Charge Your Phone in Your Pocket. In *Proceedings of the 20th Annual International Conference on Mobile Computing and Networking (MobiCom '14)*. ACM, New York, NY, USA, 495–506. https://doi.org/10.1145/2639108.2639130

[12] Farid Jolani, Yiqiang Yu, and Zhizhang Chen. 2015. A planar positioning-free magnetically-coupled resonant wireless power transfer. In *2015 IEEE Wireless Power Transfer Conference (WPTC)*. 1–3. https://doi.org/10.1109/WPT.2015.7140176

[13] Yoshihiro Kawahara, Wei Wei, Yoshiaki Narusue, Ryo Shigeta, Tohru Asami, and Manos Tentzeris. 2013. Virtualizing power cords by wireless power transmission and energy harvesting. In *2013 IEEE Radio and Wireless Symposium*. 37–39. https://doi.org/10.1109/RWS.2013.6486633

[14] Mehdi Kiani and Maysam Ghovanloo. 2012. The Circuit Theory Behind Coupled-Mode Magnetic Resonance-Based Wireless Power Transmission. *IEEE Transactions on Circuits and Systems I: Regular Papers* 59, 9 (Sept 2012), 2065–2074. https://doi.org/10.1109/TCSI.2011.2180446

[15] Sangkil Kim, Rushi Vyas, Jo Bito, Kyriaki Niotaki, Ana Collado, Apostolos Georgiadis, and Manos M Tentzeris. 2014. Ambient RF Energy-Harvesting Technologies for Self-Sustainable Standalone Wireless Sensor Platforms. *Proc. IEEE* 102, 11 (Nov 2014), 1649–1666. https://doi.org/10.1109/JPROC.2014.2357031

[16] Steven Kisseleff, Ian F Akyildiz, and W Gerstacker. 2015. Beamforming for magnetic induction based wireless power transfer systems with multiple receivers. *Proceedings of the 2015 IEEE Global Commun. Conf. (GLOBECOM)* (Dec 2015), 1–7. https://doi.org/10.1109/GLOCOM.2015.7417006

[17] Ryosuke Kobayashi, Yoshiaki Narusue, Wei Wei, Yoshihiro Kawahara, and Tohru Asami. 2014. Performance evaluation of multilevel ASK communication for a multi-hop wireless resonance system. In *2014 IEEE Wireless Power Transfer Conference*. 76–79. https://doi.org/10.1109/WPT.2014.6839598

[18] Andre Kurs, Aristeidis Karalis, Robert Moffatt, John D Joannopoulos, Peter Fisher, and Marin Soljačić. 2007. Wireless power transfer via strongly coupled magnetic resonances. *Science* 317, 5834 (2007), 83–86. https://doi.org/10.1126/science.1143254

[19] Chi Kwan Lee, Wen Xing Zhong, and SYR Hui. 2012. Effects of Magnetic Coupling of Nonadjacent Resonators on Wireless Power Domino-Resonator Systems. *IEEE Transactions on Power Electronics* 27, 4 (April 2012), 1905–1916. https://doi.org/10.1109/TPEL.2011.2169460

[20] Zhu Liu, Zhizhang David Chen, and Huapeng Zhao. 2017. A simple structure of planar transmitting array for multi-receiver wireless power reception. In *2017 IEEE Wireless Power Transfer Conference (WPTC)*. 1–2. https://doi.org/10.1109/WPT.2017.7953895

[21] Zhen Ning Low, Raul Andres Chinga, Ryan Tseng, and Jenshan Lin. 2009. Design and Test of a High-Power High-Efficiency Loosely Coupled Planar Wireless Power Transfer System. *IEEE Trans. Ind. Electron.* 56, 5 (2009), 1801–1812. https://doi.org/10.1109/TIE.2008.2010110

[22] Andrea Massa, Giacomo Oliveri, Federico Viani, and Paolo Rocca. 2013. Array Designs for Long-Distance Wireless Power Transmission: State-of-the-Art and Innovative Solutions. *Proc. IEEE* 101, 6 (June 2013), 1464–1481. https://doi.org/10.1109/JPROC.2013.2245491

[23] Hiroshi Matsumoto. 2002. Research on solar power satellites and microwave power transmission in Japan. *IEEE Microwave Magazine* 3, 4 (Dec 2002), 36–45. https://doi.org/10.1109/MMW.2002.1145674

[24] S. Abdollah Mirbozorgi, Hadi Bahrami, Mohamad Sawan, and Benoit Gosselin. 2016. A Smart Cage With Uniform Wireless Power Distribution in 3D for Enabling Long-Term Experiments With Freely Moving Animals. *IEEE Transactions on Biomedical Circuits and Systems* 10, 2 (April 2016), 424–434. https://doi.org/10.1109/TBCAS.2015.2414276

[25] Kazuaki Mori, Hyunkenun Lim, Shunta Iguchi, Koichi Ishida, Makoto Takamiya, and Takayasu Sakurai. 2012. Positioning-Free Resonant Wireless Power Transmission Sheet With Staggered Repeater Coil Array (SRCA). *IEEE Antennas and Wireless Propagation Letters* 11 (2012), 1710–1713. https://doi.org/10.1109/LAWP.2013.2239600

[26] Yoshiaki Narusue and Yoshihiro Kawahara. 2017. Distributed reactance compensation for printed spiral coils in wireless power transfer. In *2017 IEEE Wireless Power Transfer Conference (WPTC)*. 1–4. https://doi.org/10.1109/WPT.2017.7953904

[27] Yoshiaki Narusue, Yoshihiro Kawahara, and Tohru Asami. 2013. Impedance matching method for any-hop straight wireless power transmission using magnetic resonance. In *2013 IEEE Radio and Wireless Symposium*. 193–195. https://doi.org/10.1109/RWS.2013.6486685

[28] Yoshiaki Narusue, Yoshihiro Kawahara, and Tohru Asami. 2017. Maximizing the efficiency of wireless power transfer with a receiver-side switching voltage regulator. *Wireless Power Transfer* 4, 1 (2017), 42–54. https://doi.org/10.1017/wpt.2016.14

[29] Aaron N. Parks, Alanson P. Sample, Yi Zhao, and Joshua R. Smith. 2013. A wireless sensing platform utilizing ambient RF energy. In *2013 IEEE Topical Conference on Biomedical Wireless Technologies, Networks, and Sensing Systems*. 154–156. https://doi.org/10.1109/BioWireleSS.2013.6613706

[30] Gregory M. Plaizier, Erik Andersen, Binh Truong, Xiang He, Shad Roundy, and Kam K. Leang. 2018. Design, Modeling, and Analysis of Inductive Resonant Coupling Wireless Power Transfer for Micro Aerial Vehicles (MAVs). In *2018 IEEE International Conference on Robotics and Automation (ICRA)*. 1–6. https://doi.org/10.1109/ICRA.2018.8461162

[31] David S Ricketts, Matthew J Chabalko, and Andrew Hillenius. 2013. Experimental demonstration of the equivalence of inductive and strongly coupled magnetic resonance wireless power transfer. *Applied Physics Letters* 102, 5 (January 2013), 053904. https://doi.org/10.1063/1.4788748

[32] Alanson P Sample, David T Meyer, and Joshua R Smith. 2011. Analysis, experimental results, and range adaptation of magnetically coupled resonators for wireless power transfer. *IEEE Transactions on Industrial Electronics* 58, 2 (March 2011), 544–554. https://doi.org/10.1109/TIE.2010.2046002

[33] Alanson P Sample, Benjamin H Waters, Scott T Wisdom, and Joshua R Smith. 2013. Enabling Seamless Wireless Power Delivery in Dynamic Environments. *Proc. IEEE* 101, 6 (June 2013), 1343–1358. https://doi.org/10.1109/JPROC.2013.2252453

[34] Alanson P Sample, Daniel J Yeager, Pauline S Powledge, Alexander V Mamishev, and Joshua R Smith. 2008. Design of an RFID-based battery-free programmable sensing platform. *IEEE Transactions on Instrumentation and Measurement* 57, 11 (June 2008), 2608–2615. https://doi.org/10.1109/TIM.2008.925019

[35] Susumu Sasaki, Koji Tanaka, and Kenichiro Maki. 2013. Microwave Power Transmission Technologies for Solar Power Satellites. *Proc. IEEE* 101, 6 (June 2013), 1438–1447. https://doi.org/10.1109/JPROC.2013.2246851

[36] Takuya Sasatani, Matthew J Chabalko, Yoshihiro Kawahara, and Alanson P Sample. 2017. Multimode Quasistatic Cavity Resonators for Wireless Power Transfer. *IEEE Antennas Wireless Propagation Letters* 16 (August 2017), 2746–2749. https://doi.org/10.1109/LAWP.2017.2744658

[37] Takuya Sasatani, Chouchang Jack Yang, Matthew J. Chabalko, Yoshihiro Kawahara, and Alanson P. Sample. 2018. Room-Wide Wireless Charging and Load-Modulation Communication via Quasistatic Cavity Resonance. *Proc. ACM Interact. Mob. Wearable Ubiquitous Technol.*

2, 4, Article 188 (Dec. 2018), 23 pages. https://doi.org/10.1145/3287066
[38] James Scott, Frank Hoffmann, Michael D. Addlesee, Glenford Mapp, and Andy Hopper. 2002. Networked Surfaces: A New Concept In Mobile Networking. *ACM Mobile Networks and Applications* 7, No. 5, 353–364. https://doi.org/10.1109/MCSA.2000.895377
[39] Tsuyoshi Sekitani, Makoto Takamiya, Yoshiaki Noguchi, Shintaro Nakano, Yusaku Kato, Takayasu Sakurai, and Takao Someya. 2007. A large-area wireless power-transmission sheet using printed organic transistors and plastic MEMS switches. *Nature materials* 6, 6 (2007), 413. https://doi.org/doi:10.1038/nmat1903
[40] Lixin Shi, Zachary Kabelac, Dina Katabi, and David Perreault. 2015. Wireless Power Hotspot That Charges All of Your Devices. In *Proceedings of the 21st Annual International Conference on Mobile Computing and Networking (MobiCom '15)*. ACM, New York, NY, USA, 2–13. https://doi.org/10.1145/2789168.2790092
[41] Xingyi Shi and Joshua R. Smith. 2016. Large area wireless power via a planar array of coupled resonators. In *2016 International Workshop on Antenna Technology (iWAT)*. 200–203. https://doi.org/10.1109/IWAT.2016.7434842
[42] Ryo Shigeta, Tatsuya Sasaki, Duong M. Quan, Yoshihiro Kawahara, Rushi J. Vyas, Manos M. Tentzeris, and Tohru Asami. 2013. Ambient RF Energy Harvesting Sensor Device With Capacitor-Leakage-Aware Duty Cycle Control. *IEEE Sensors Journal* 13, 8 (Aug 2013), 2973–2983. https://doi.org/10.1109/JSEN.2013.2264931
[43] Jaegue Shin, Seungyong Shin, Yangsu Kim, Seungyoung Ahn, Seokhwan Lee, Guho Jung, Seong-Jeub Jeon, and Dong-Ho Cho. 2014. Design and implementation of shaped magnetic-resonance-based wireless power transfer system for roadway-powered moving electric vehicles. *IEEE Trans. Ind. Electron.* 61, 3 (2014), 1179–1192. https://doi.org/10.1109/TIE.2013.2258294
[44] Naoki Shinohara. 2011. Power without wires. *IEEE Microwave Magazine* 12, 7 (Dec 2011), S64–S73. https://doi.org/10.1109/MMM.2011.942732
[45] Naoki Shinohara and Shigeo Kawasaki. 2009. Recent Wireless Power Transmission technologies in Japan for space solar power station/satellite. In *2009 IEEE Radio and Wireless Symposium*. 13–15. https://doi.org/10.1109/RWS.2009.4957272
[46] Naoki Shinohara, Tomohiko Mitani, and Hiroshi Matsumoto. 2005. Study on ubiquitous power source with microwave power transmission. In *Proc. URSI General Assembly*. C07.
[47] Ryo Takahashi, Takuya Sasatani, Fuminori Okuya, Yoshiaki Narusue, and Yoshihiro Kawahara. 2018. A Cuttable Wireless Power Transfer Sheet. *Proc. ACM Interact. Mob. Wearable Ubiquitous Technol.* 2, 4, Article 190 (Dec. 2018), 25 pages. https://doi.org/10.1145/3287068
[48] Makoto Takamiya, Tsuyoshi Sekitani, Yoshio Miyamoto, Yoshiaki Noguchi, Hiroshi Kawaguchi, Takao Someya, and Takayasu Sakurai. 2007. Design Solutions for a Multi-Object Wireless Power Transmission Sheet Based on Plastic Switches. In *2007 IEEE International Solid-State Circuits Conference. Digest of Technical Papers*. 362–609. https://doi.org/10.1109/ISSCC.2007.373444
[49] Vamsi Talla, Bryce Kellogg, Shyamnath Gollakota, and Joshua R. Smith. 2017. Battery-Free Cellphone. *Proceedings of the ACM on Interactive, Mobile, Wearable and Ubiquitous Technologies (IMWUT)* 1, 2, Article 25 (June 2017), 20 pages. https://doi.org/10.1145/3090090
[50] Dries Van Wageningen and Toine Staring. 2010. The Qi wireless power standard. In *Proceedings of the 2010 14th International Power Electronics and Motion Control Conference (EPE/PEMC)*. IEEE, S15–25. https://doi.org/10.1109/EPEPEMC.2010.5606673
[51] Bingnan Wang, William Yerazunis, and Koon Hoo Teo. 2013. Wireless Power Transfer: Metamaterials and Array of Coupled Resonators. *Proc. IEEE* 101, 6 (June 2013), 1359–1368. https://doi.org/10.1109/JPROC.2013.2245611
[52] Benjamin H. Waters, Brody J. Mahoney, Vaishnavi Ranganathan, and Joshua R. Smith. 2015. Power Delivery and Leakage Field Control Using an Adaptive Phased Array Wireless Power System. *IEEE Transactions on Power Electronics* 30, 11 (Nov 2015), 6298–6309. https://doi.org/10.1109/TPEL.2015.2406673
[53] Benjamin H. Waters, Alanson P. Sample, Pramod Bonde, and Joshua R. Smith. 2012. Powering a Ventricular Assist Device (VAD) With the Free-Range Resonant Electrical Energy Delivery (FREE-D) System. *Proc. IEEE* 100, 1 (Jan 2012), 138–149. https://doi.org/10.1109/JPROC.2011.2165309
[54] Xiu Zhang, SL Ho, and WN Fu. 2012. Quantitative Design and Analysis of Relay Resonators in Wireless Power Transfer System. *IEEE Transactions on Magnetics* 48, 11 (Nov 2012), 4026–4029. https://doi.org/10.1109/TMAG.2012.2202883
[55] Wenxing Zhong, Chi Kwan Lee, and SY Ron Hui. 2013. General Analysis on the Use of Tesla's Resonators in Domino Forms for Wireless Power Transfer. *IEEE Transactions on Industrial Electronics* 60, 1 (Jan 2013), 261–270. https://doi.org/10.1109/TIE.2011.2171176

Received August 2018; revised February 2019; accepted June 2019